

# **Review of Aeronautical Fatigue Investigations in Switzerland**

**May 2003 – April 2005**

**KOR-TA2005-0252**

**M. Guillaume  
RUAG Aerospace  
CH- 6032 Emmen**

## **SUMMARY**

The Swiss review summarizes fatigue work in Switzerland. It includes main contributions from the RUAG Aerospace (RA), CFS Engineering, and Pilatus Aircraft Ltd. This document later forms a chapter of the ICAF conference minutes published by the conference host nation. The format of the review reflects ICAF requirements.

Prepared for the presentation at the 29<sup>th</sup> ICAF Conference  
Hamburg, 06 and 07 June 2005

SUMMARY .....	1
4.1 INTRODUCTION.....	3
4.2 STATUS OF THE SWISS F/A-18 FULL SCALE FATIGUE TEST .....	4
4.2.1 Introduction .....	4
4.2.2 Loading Program.....	4
4.2.3 Loading System.....	4
4.2.4 Measurement Data.....	5
4.2.5 Inspections.....	7
4.2.6 Test Performance.....	7
4.2.7 Final Inspection Program .....	9
4.2.8 Tear Down Inspection Program .....	9
4.2.9 Structural Findings during the Test.....	9
4.3 NEW MEASUREMENT TECHNOLOGY FOR DISPLACEMENT.....	20
4.4 FATIGUE LOADS DEVELOPMENT USING COMPUTATIONAL FLUID DYNAMICS.....	23
4.4.1 Technology of Computational Fluid Dynamics .....	23
4.5 FATIGUE RELATED TOPICS ON MILITARY AIRCRAFT.....	27
4.5.1 Development of a Procedure to Calculate Aircraft Balanced Load Distribution for Swiss F/A-18 Service Flights .....	27
4.5.2 F/A-18, SLP, Load to Stress.....	28
4.5.3 Development of Swiss F/A-18 Pegging Procedure.....	30
4.5.4 Damage Investigation on F-5 Horizontal Stabilizer.....	33
4.6 FATIGUE RELATED APPLIED RESEARCH AND DEVELOPMENT .....	36
4.6.1 Repair Welding of Titanium Parts .....	36
4.6.2 Fatigue Behavior of Metals and Residual Stresses .....	40
4.6.3 Automated Crack Detection by Crack Sensor.....	41
4.7. FULL SCALE FATIGUE TEST OF THE PILATUS PC-21 AIRCRAFT .....	44
4.7.1 Introduction .....	44
4.7.2 Full Scale Fatigue Test Program .....	44

## 4.1 INTRODUCTION

The present review gives a brief summary of the work performed in Switzerland in the field of aeronautical fatigue, during the period from May 2003 till April 2005. The various contributions to this review come from the following sources:

- RUAG Aerospace; Fatigue Engineering, Aerodynamic, and Full Scale Fatigue Test Project Team
- Pilatus Aircraft Ltd; Structural Engineering
- CFS Engineering, Lausanne
- M@M GmbH

The work of fatigue related topics on military aircraft was supported by Michel Godinat, Andrea Oswald, Yann Fasel, Stefan Oesch, and Jan Weiss. Their effort is gratefully acknowledged.

A part of the preparation of this review is sponsored by the armasuisse. This fund is gratefully acknowledged.

## 4.2 STATUS OF THE SWISS F/A-18 FULL SCALE FATIGUE TEST

M. Guillaume, I. Pfiffner, L. Schmid, RUAG Aerospace

### 4.2.1 Introduction

Swiss Air Force requirements are that the F/A-18C/D aircraft can be operated for 30 years and for 5'000 flight hours (FH) under Swiss usage conditions. Since the Swiss F/A-18 usage spectrum was found to be more severe than the design usage spectrum of the US Navy F/A-18 aircraft, critical parts of the Swiss F/A-18 structure had to be redesigned at the time of the procurement of the aircraft. For the same reason, however, the US Navy qualification tests for the US Navy F/A-18 structure do not cover Swiss requirements. Therefore a Full Scale Fatigue Test (FSFT) must be performed, in order to validate the Swiss F/A-18C/D structural design and to qualify the design service life of the aircraft. Since it was not possible to perform a FSFT prior to the production of the Swiss aircraft, obviously, the test results will not lead to further improvement of the structural design. Instead, emphasis is given to a test, which will also support an economical maintenance and a high availability of the structure of Swiss F/A-18C/D fleet aircraft.

The Swiss FSFT is unique due to the fact that a double-seated F/A-18D configuration was tested.

### 4.2.2 Loading Program

In order to demonstrate compliance with the service life of 5'000 FH a scatter factor of 2 is employed. An additional 400 FH of fatigue cycling are scheduled to account for residual strength capability based on damage tolerance studies. In total, 10'400 FH were simulated in the Swiss test. A truncated Master Event Spectrum for the Swiss fatigue test (Test-MES) was generated, which was already published in the previous National Reviews. All fatigue loads were derived from maneuver component loads. The Test-MES consists of 26'990 load lines with 2'009 unique flight load cases (excluding cockpit pressure) representing a block of 200 flight hours. During each flight two full cockpit pressure cycles were applied.

### 4.2.3 Loading System

Altogether 68 hydraulic actuators were installed into the test rig to simulate air and inertia loads (see Figure 4.2-1, yellow). The actuators are distributed over the aircraft in the following manner:

- Fuselage 20 jacks
- Wing box and flaps (L/H, R/H): 16 + 16 jacks
- Leading Edge Extension (LEX): 3 + 3 jacks
- Empennage (Vertical, Horizontal): 4 + 6 jacks

### Restraint System:

The test article is restrained by six single struts in a statically determined manner:

- Vertical direction: Nose (1) and main landing gear (2)
- Lateral direction: Forward fuselage (1) and arresting hook dummy (1)
- Flight direction: Engine dummies (1)



Figure 4.2-1 Test set-up of the Swiss full scale fatigue test.

### 4.2.4 Measurement Data

#### Static strain survey data:

Static measurements are understood to provide health monitoring for both the ~1'100 strain gauges and the structure. Also, they allow each strain gauge to be surveyed and to be classified by functionality, linearity, reliability and hysteresis effects.

Furthermore, strain survey data is used for reference purposes in the crack initiation computation.

The static strain surveys (Figure 4.2-2) are characterized by:

- Performance of seven load cases with maximum loads (e.g. wing root bending).
- Ramping up of the single load cases up to 70% load level in steps of 10%.
- Measurement of all strain gauges at each load level.
- Regular strain surveys in intervals of 1'000 FH.
- Additional strain surveys in case of major repairs and longer down time.

Continuous measurement data:

During fatigue cycling approx. 300 data channels were recorded with a sampling rate of 10 Hz. After being filtered with a rise/fall criteria the strain spectrum data was used for crack initiation computation.

Additionally instrumented strain gauges were measured continuously in order to obtain strain spectra for these gauges. Also, continuous measurements allow close monitoring of strain gauges, however, the limited availability of channels prohibits strain spectrum measurements of all strain gauges.



Figure 4.2-2 Wing displacement during strain survey at 70% load level of  $N_z = 8.25g$  symmetric steady state pull up maneuver.

Unique load cases measurement:

At 1'000 FH a special measurement campaign was performed to establish a strain spectrum for each strain gauge. These strain spectra were used extensively for data analysis, whereas a Boeing crack initiation software package (CI89 software) is employed widely.

The unique load cases measurement program can be broken down into two steps:

- All 2011 unique load cases of the loading program are run one by one each followed by a mass compensation load case (0g).
- The recorded data is post-processed such that the strain spectra correspond to ordinary 26'990 line-by-line spectra.

### 4.2.5 Inspections

The inspection concept was based on the Swiss ASIP study performed around 1990. Generally the Swiss redesigned parts, parts with manufacturing flaws and test specific items (e.g. load introduction locations) were considered.

Due to the optimal accessibility the test article was inspected visually by qualified staff in daily walk-around inspections during the fatigue cycling, see Figure 4.2-3. Also the dorsal deck, the engine bay, the engine inlet, the bulkheads on the lower side were inspected for early cracks.



Figure 4.2-3 Inspection at wing fold during fatigue cycling, see deflected wing.

Major inspections were scheduled in intervals of 1'000 FH. After the removal of covers and selected bolts detailed visual inspections, eddy current inspections, and ultrasonic inspections were performed. On the upper wing surface some bolts were removed to get access to the inner wing structure for the videoscope sensor. The critical locations at the closure rib, the kick rib, and at the spars and ribs could be monitored to get early information on potential fatigue damaged structure.

### 4.2.6 Test Performance

During the commissioning phase the test system was optimized and the cycling speed increased significantly, so that it only takes about 18 hours to simulate 200 FH. By working in shifts 1'000 FH could be completed within a work week. The test facility could be operated by one single engineer. Since the test started in January 2003 the test article logged already 5'000 FH (one service life) by June 2003.

At 5'000 FH the test was stopped for the performance of a complete inspection. For this purpose covers on the fuselage and the wing were removed to get more access to the inner structure of the center fuselage and wing. The inner, and outer wing, as well as all the flaps were not removed. This inspection was a major milestone in the test program. No fatigue damage was observed at fracture critical locations. The simulation of 5'000 FH corresponds already to more than 16'000 FH on the US Navy test FT01/ST16/FT93.

The test was resumed in September 2003 for the second life time. A short inspection after 500 FH was introduced starting at 7'500 FH. The test was stopped for half a day to inspect some areas in more detail. The cover of tank #4 was removed for doing inspections in the aft section of the center fuselage which was heavily loaded in our test.

Due to the replacement of the outboard TEF hinge rib at 6'450 FH the test has to be stopped from November 2003 till March 2004.

A further stop was needed to reinforce the upper outboard longeron on the L/H side by a strap in April 2004. The longeron was severely cracked in the aft section of the center fuselage.

The wing fold transmission had to be replaced at 4'000 FH. The wing fold transmission is a life limited part. During the Swiss ASIP study a safe life of 4'000 FH was assumed by Boeing. Therefore two spare sets of transmission were provided by Boeing for the Swiss test.

At 9'181 FH and 9'461 FH the ILEF were replaced by scrapped Canadian ILEF to continue the test. The Swiss ILEF showed a disbonding failure at the lug area due to the large cracks in the outer lug set. RUAG maintenance people were able to replace this ILEF flap within a day and to resume the test again.

The Swiss test reached the 10'400 FH in September 2004 in less then two years, see Figure 4.2-4. The test article sustained the last strain survey which any problems. The structure was still able to carry the load of a 9g steady state limit load condition.

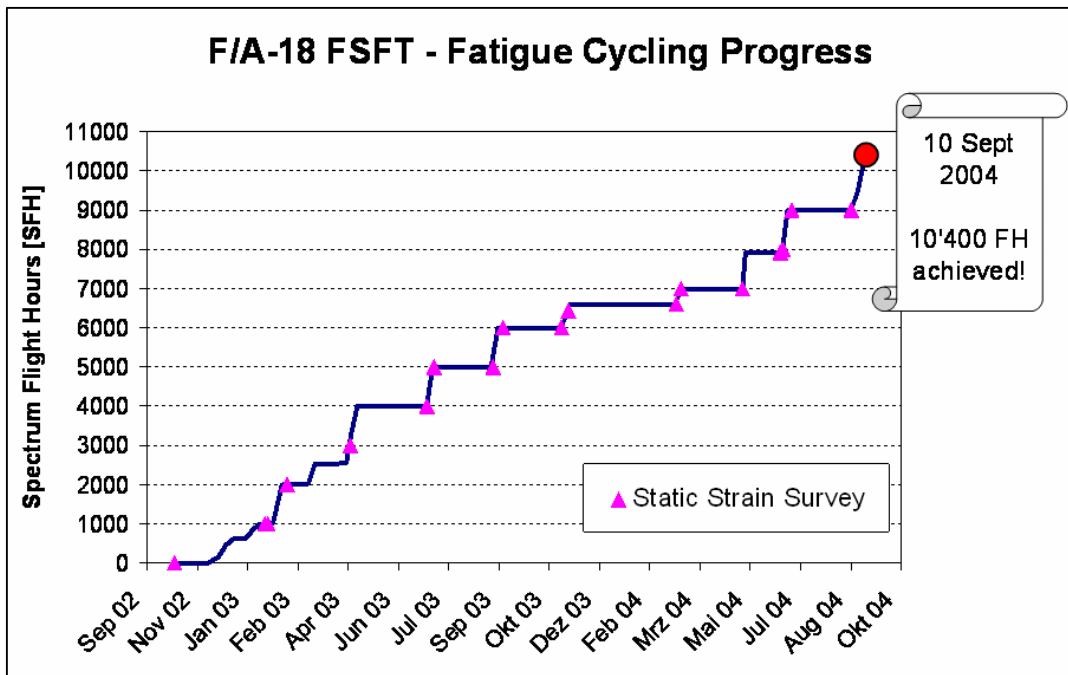


Figure 4.2-4 Fatigue cycling progress to reach 10'400 FH.

#### **4.2.7 Final Inspection Program**

After completion of the 10'400 FH in September 2004 the test article was inspected in detail in similar way as after 5'000 FH. In the first instances all non conformances observed during the fatigue cycling were inspected. In a second step all the flaps, the outer wing, and the FREE LEX were dismantled and all the interfaces were properly checked for non conformances during cycling.

In January 2005 the inner wing was removed from the fuselage and the complete airplane was removed from the loading rig. In March 2005 the final inspection was completed with the delivery of the final report to armasuisse with all the non conformances of the Swiss full scale fatigue test.

#### **4.2.8 Tear Down Inspection Program**

First discussions were initiated already in Summer 2003 between armasuisse and the project management to discuss the next steps after the test completion. Several options were considered and discussed in detail:

- Disassembly of the test rig and storage of the test article
- Performance of a 9g static test
- Continuation of the fatigue cycling of a third or fourth life time
- Disassembly of the test rig and performance of tear down inspection

In March 2004 in a management meeting together with armasuisse it was decided to disassemble the test article and do a limited tear down inspection which should last three years. This option offered the best value for the limited budget.

Within two months the whole test set up was dismantled and first steps could be started in April 2005 for the teardown inspection. The goal is to tear down the center fuselage and the R/H wing which is a wing with non conformances of the Swiss production.

#### **4.2.9 Structural Findings during the Test**

*Cracks at Inboard Leading Edge Flap (ILEF):*

The ILEF was analyzed in the Swiss ASIP study. Due to cracks at the lower lug area in the FT93 wing test the Swiss ILEF was redesigned (Figure 4.2-5 a, b). The Swiss configuration was changed from circular fillets at the lug area to parabolic fillets. Furthermore for the forward and aft lug of the inboard lug set the thickness was increased by 50%. The spar web was moved forward compared to the US Navy design. The Swiss improvements showed by analysis a crack initiation life of 38'000 FH based on the hinge moment spectrum.

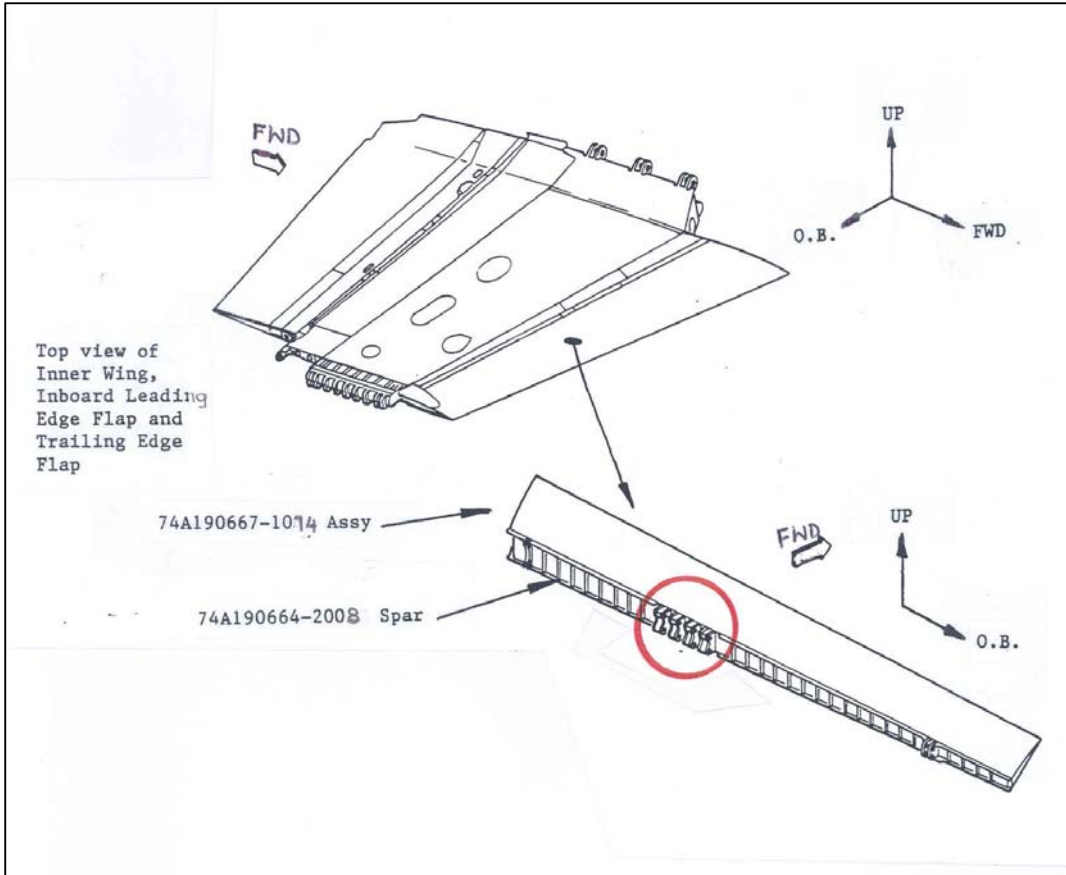


Figure 4.1-5 a Overview of the inner wing with the ILEF flap and the lug area.

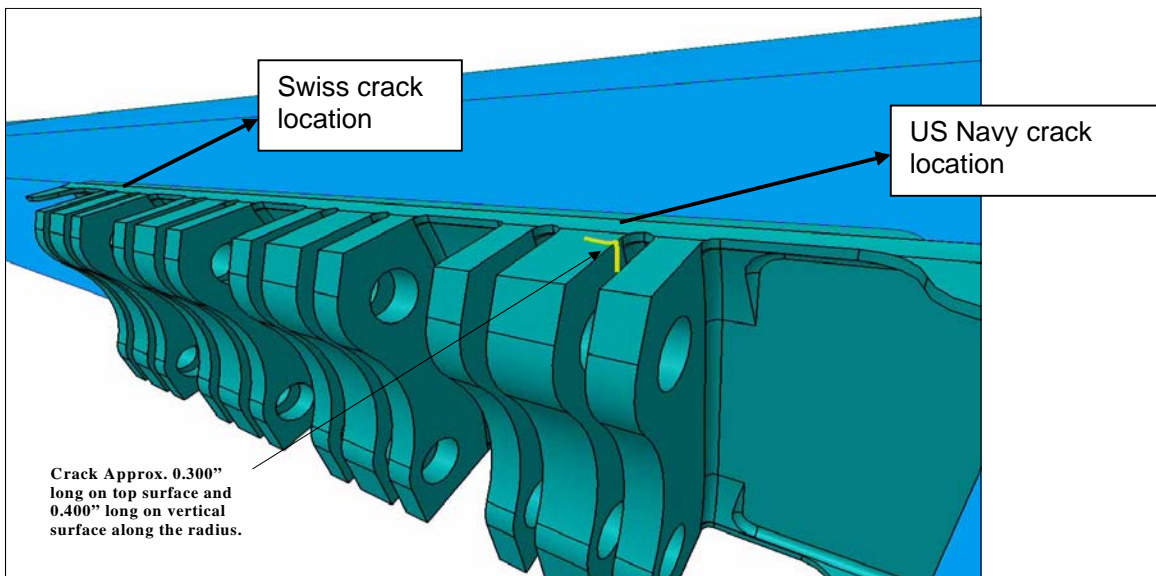


Figure 4.1-5 b Cracks observed at ILEF lower lug fillets on FT93 wing test and on Swiss test article.

In our test the ILEF is loaded by two actuators with tension/compression "whiffletrees" from the underside. With this layout a fixed center of pressure (CP) is simulated. For every load case the correct hinge moment is simulated according to the loads developed in the ASIP study. The deflection angle of the ILEF is set to  $0^\circ$  (fixed position).

In the Swiss FSFT at 3'000 FH a crack was observed in the most outboard lug at the lower side (Figure 4.2-6). The crack was not perpendicular to the lug load as in the FT93 wing test, rather it runs  $30^\circ$  off into the spar web and the spar flange.

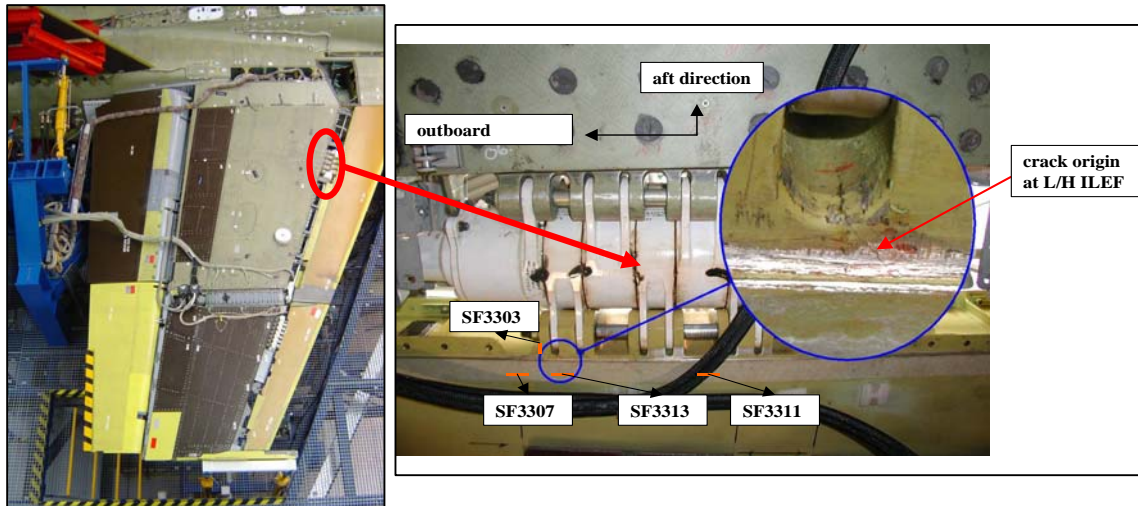


Figure 4.2-6 Swiss crack observed at 3'000 FH on the lower side of the ILEF lug fillet area; the strain gauge locations are labeled orange (application at 4'000 FH).

To get a better understanding of the loading at the lug area overall 16 additional strain gauges were applied. All these gauges were continuously monitored during the fatigue cycling.

The curvature of the ILEF spar was determined in three ways: three point loading constraint, the full FSFT FE model, and from strain gauge data. All the numbers agree well, which indicates that the ILEF spar deflection is influenced heavily by inner wing bending.

Under span-wise loading the parabolic fillet has an adverse effect on local stresses, whereas the lug loading is reduced.

The strain survey results up to 6'000 FH showed significant changes in the area close to the crack. The strain gauges at lug set #1, #2, and #3, however, do only see minor changes due to the growing crack in the spar section.

From continuous measurements of the 16 strain gauges crack initiation curves (CI) were generated. The CI curves at the lug affected trough the crack showed a drift to lower stress levels which demonstrates the growing crack in the spar. The CI curves do not show any drift for the gauges at lug set #1, #2, and #3.

The crack grew in direction of the neutral axis and it was inspected regularly during fatigue cycling. Due to the opening of the crack the bonded skin of the ILEF started to disbond. First data of disbonding area was monitored at 7'000 FH using ultrasonic inspection. At 7'236 FH a crack was observed at the corner of the outboard lug, see Figure 4.2-7. This crack grew

further and merged with the original crack observed at 3'000 FH. The ILEF skin failed at 9'181 FH (R/H side) and at 9'461 FH (L/H side). They were replaced by Canadian scrapped ILEF (US Navy configuration) for the rest of the test.

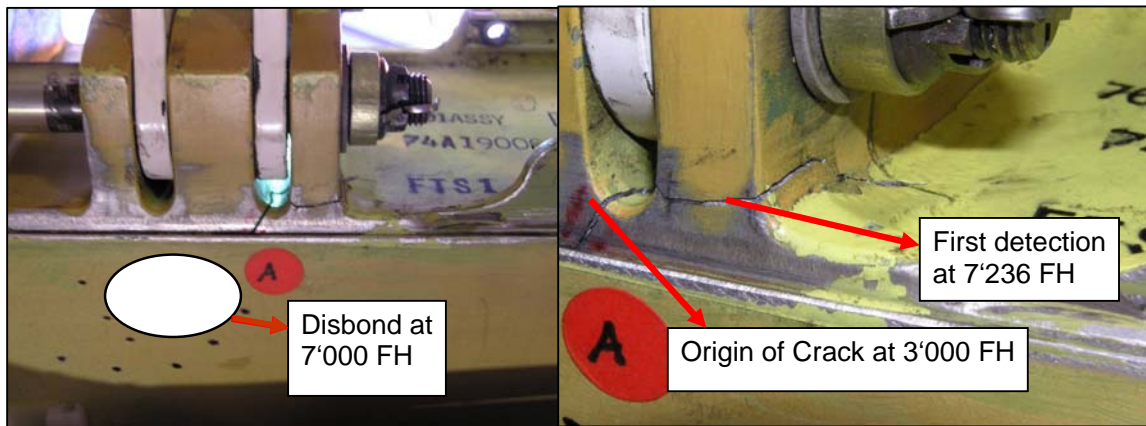


Figure 4.2-7 Cracks at ILEF observed on Swiss test, status at 9'000 FH.

*Cracks at inner wing front spar lug drive area:*

At 9'000 FH a crack was observed at the lower side of lug area of front spar in the main transmission drive area, see Figure 4.2-8. The crack was along the lug fillet direction and on the lower surface. The crack was running along a mechanical drill mark along the fillet direction. This damage was only observed on L/H side. Up to 10'400 FH the crack grew further but the crack growth rate was relatively slow. At 9'464 FH an additional crack was observed on other lug fillet. The crack runs also along a mechanical drill mark and the crack growth rate was small up to 10'400 FH. No drill marks were observed on R/H side and no damage was found up to 10'400 FH.

Drill marks and residual stresses due to machining in such areas as lug fillet may have a detrimental impact on the fatigue life of these parts.

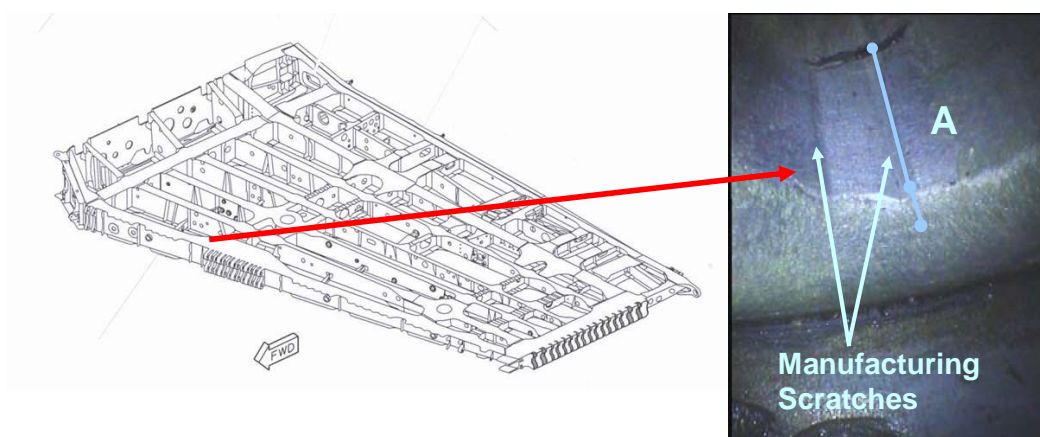


Figure 4.2-8 Crack in the lower lug area of the inner wing front spar due to manufacturing scratches.

*Cracks at wing fold transmission and at outer wing fold rib:*

The F/A-18 is an airplane designed for the US Navy for carrier operations. Therefore the outer wing can be folded by a transmission mechanism (Figure 4.2-9). The titanium wing fold ribs at the inner and outer wing transfer the loads through the transmission. The inner and outer wing fold ribs are highly loaded and fracture critical parts.



Figure 4.2-9 Wing fold mechanism for the F/A-18.

Additionally to the strain gauge measurements during a strain survey also displacement measurements are done at 14 different locations with wire transmitting potentiometers. During fatigue cycling a max up displacement (9g symmetrical maneuver) of +20.5 inch and a max down displacement (-2g symmetrical maneuver) of -9.5 inch at the wing tip was observed.

*The static displacements versus the load showed the following behavior:*

The increase of the displacement can be very well approximated with a straight line. However this line does not cross necessarily the origin, it means that the load must sometimes overcome some free play before the structure reaches a linear behavior.

The displacements were analyzed after every 1'000 FH (during every strain survey) and the following conclusions could be made:

- The structural stiffness illustrated by the linear part of the deflection versus load behavior corresponds fairly well to the prediction calculated with the FE model (internal loads model) of the overall aircraft. The real stiffness measured at the wing tip is slightly lower and the forward fuselage is in reality clearly stiffer than predicted.

- No real change of the stiffness could be observed from one strain survey to the other in any part of the test article. Small differences were measured at locations with small amplitude due to a limited resolution of the measuring system.
- The evolution of the free play in the wing displacement and particularly at the wing tip indicates a clear increasing trend. The wing fold mechanism undergoes a very rapid wear in the small gears, shown by the free play going up between 0 and 3'000 FH. In fact at 4'000 FH the fold system had to be replaced with a new one and the free play remained after that stable until 6'000 FH. A change was then observed between 6'000 and 7'000 FH and effectively the fold system had to be replaced once more after 8'000 FH.

The transmission of the wing fold rib is a life limited part. Boeing has delivered three pairs of transmissions for the Swiss test due to the limited life of approximately 4'000 FH. This limit was only estimated due to the design spectrum severity between US Navy and Swiss. Indeed after 4'000 FH of cycling the first pair of transmission showed severe cracking and had to be replaced. The weakest point is gear section 18 and 19 at the aft section which is highly loaded. At 4'000 FH also the housing of the transmission was cracked. During the continuation of the test at 6'606 FH the transmission were checked by folding the outer wing. The right hand transmission could not be folded and was therefore disassembled for detailed inspection. Several gears at the critical section 18 and 19 were already cracked. The cracked gears were replaced and the transmission was tested and adjusted. This transmission was again installed for continuation of the test. At 7'929 FH a fatale failure on this transmission was observed. The transmission could only be dismantled by breaking up the housing. The Figure 4.2-10 shows the cracked gears at the gear section 18.



Figure 4.2-10 Cracks observed at wing fold transmission section 18.

The accurate measurements of the span-wise wing deflection using displacement transducers allowed to evaluate the over testing due to the heads (rod end) of the jacks loading the outer wing (see Figure 4.2-11). The distance between the wing middle plane and the application points of the jack forces (rod end) was relatively large in the test set-up. Inevitably, by the

vertical motion of the jack head (rod end) a small lateral displacement was induced. This way the distance between the force vector and the load reference point of the wing fold was slightly increased and yields to an increase of the actual bending moment.

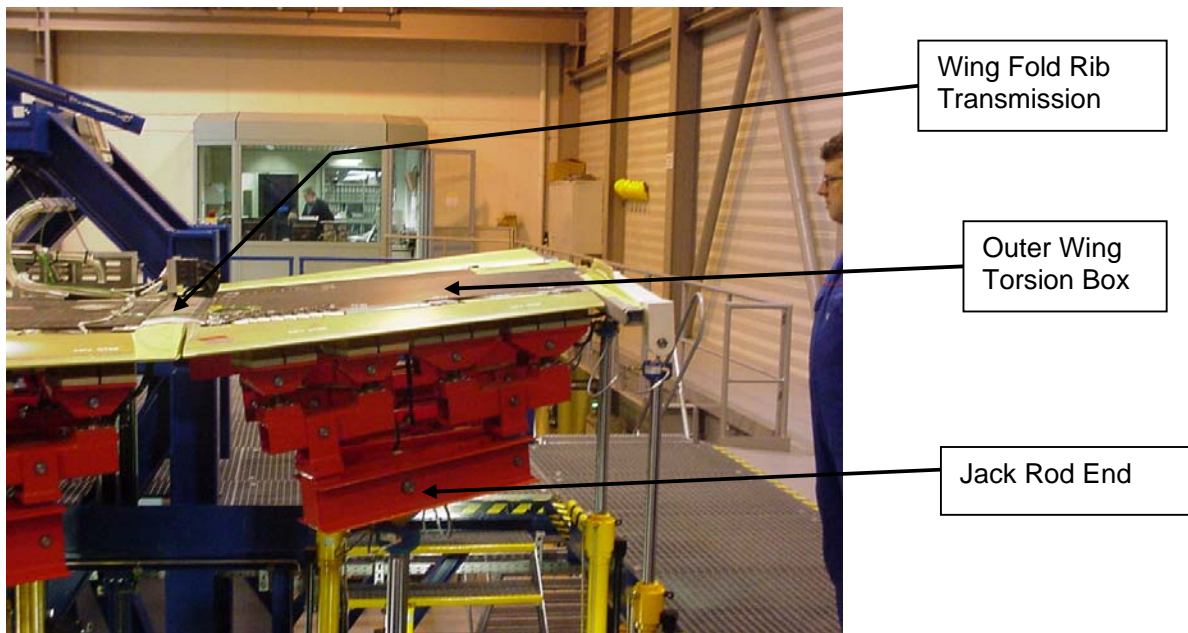


Figure 4.2-11 Displacement of rod end of the actuator at the outer wing.

For the load cases with high deflection (high g maneuvers) this increase reaches approx. 18%. A bending moment spectrum taking into account this higher loading showed clearly that this effect could absolutely not be neglected in terms of fatigue. For a relevant stress range of 110 to 130 ksi a CI-life reduction of a factor of approx. 3 was determined for the critical lug fillets at the wing fold rib. Therefore the test showed a higher severity compared to the Swiss design at the wing fold area.

The early cracking of the wing fold transmissions is not a surprise due to the severe testing of the wing fold area compared to the Swiss design. The Swiss test showed that actually the wing fold transmission seems to have more margin of safety than estimated during the ASIP study.

The forward and aft wing fold rib lugs of each lug set were beefed up (increase of the thickness) and the fillet was changed from circular to parabolic for the Swiss F/A-18 as for the ILEF. Only at one lug set #9 of the R/H outer wing fold rib a crack was observed at 6'606 FH. The crack showed small crack growth behavior. At 9'000 FH also a crack on L/H outer wing fold rib was observed. At 10'000 FH further cracks on the L/H side at lug set # 1, #5, and #8 were observed. No cracks were observed during the test at the inner wing fold rib. In the US Navy test FT01/ST16/FT93 severe cracking at inner and outer wing fold rib lugs were observed. Due to the severe testing in Swiss test compared to the Swiss ASIP design the wing fold rib seems to be superior. Even the early crack on R/H outer wing fold rib (Figure 4.2-12) did not reach the critical crack length until the end of the test. The Swiss test demonstrated that the redesigned structure can tolerate a much larger crack size than assumed in the Swiss ASIP study.

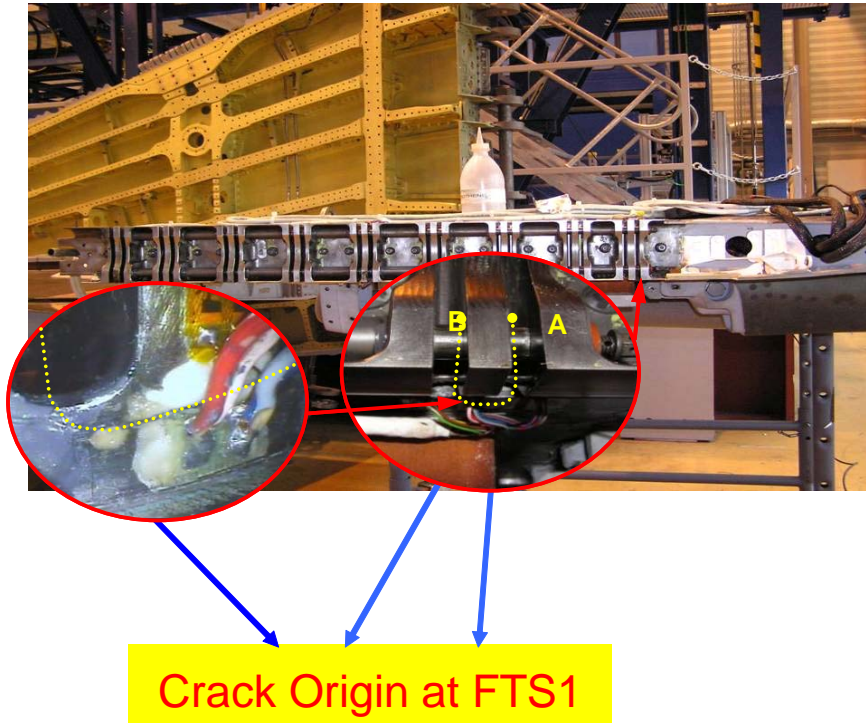


Figure 4.2-12 Observed crack at R/H outer wing fold rib lug fillet.

*Cracks in the fuel skin barrier web in the aft section of the center fuselage:*

During the inspection after the first life time at 5'000 FH the tank #4 was inspected. In the fuel barrier web skin at frame station FS526 a large crack (approx. 10 inch) was observed, see Figure 4.2-13. At 6'000 FH a large doubler was installed to avoid unloading and further damage in this area. At 7'921 FH the same crack was observed at the L/H side, the same doubler was installed. The loading on the L/H and R/H side is the same, this was confirmed by the applied loads and strain gauge readings during strain survey and the fatigue cycling. The skin thickness of the fuel barrier web skin was on the R/H side on the lower tolerance and on the L/H side on the upper tolerance of the blue print value. Further cracks were observed on the fuel skin barrier web between frame station FS97 and FS44. At 9'000 FH the doubler at the R/H side was removed because further damage at web in this area was observed. A new doubler from FS08 to FS26 was installed. The heavy loading due to horizontal tail loading is the main driver of these cracks. A loads survey of the ASIP loads procedure with using Computational Fluid Dynamics showed that the ASIP loads for the horizontal tail and the balancing procedure are not fully consistent. The aft fuselage loading of a flying F/A-18 seems to be different compared to the ASIP design loads.

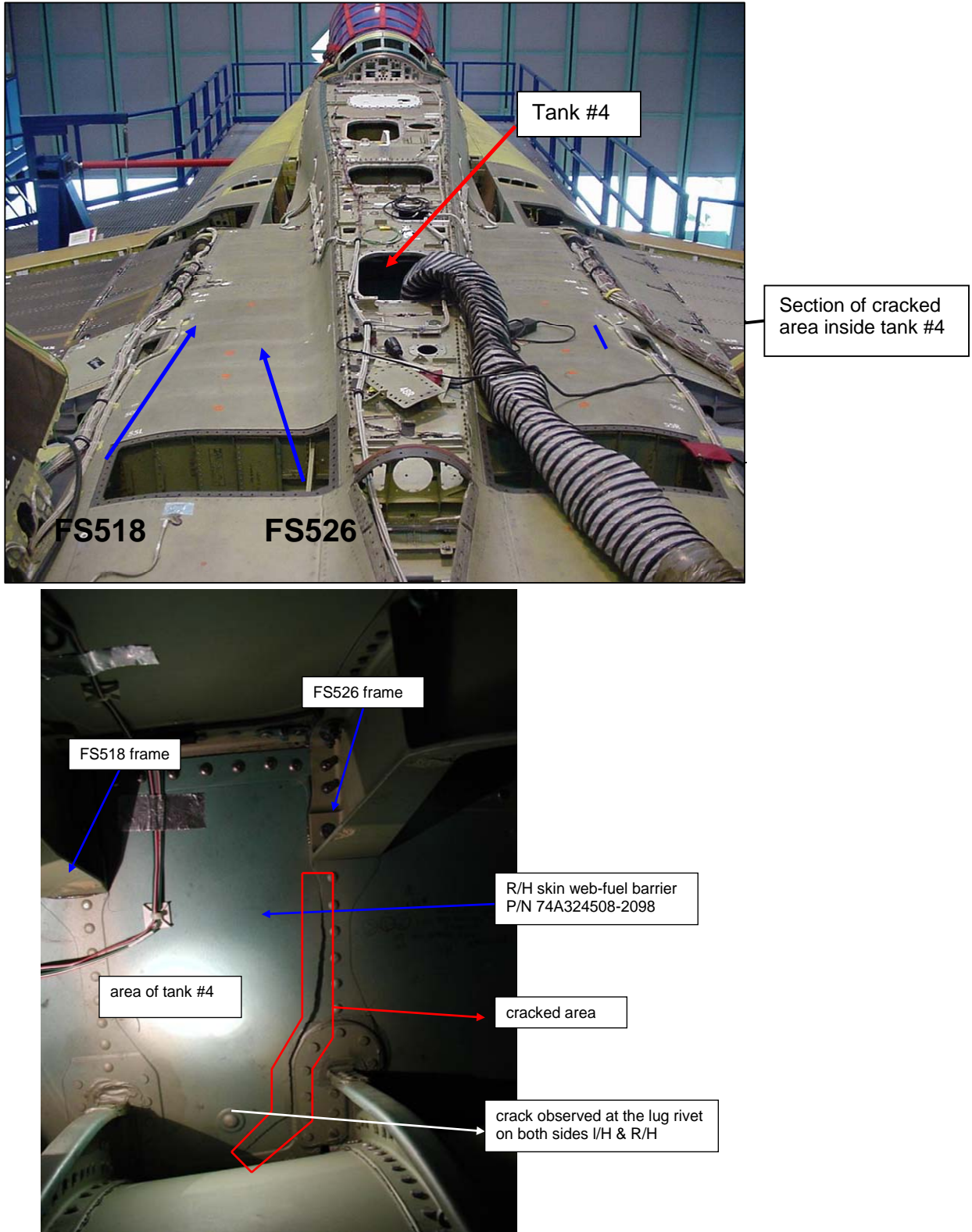


Figure 4.2-13 Observed cracks in fuel barrier web skin between FS518 and FS526.

*Cracks in the upper outboard longeron:*

During the inspection at 7'921 FH in the fuel barrier web skin at FS499 a crack was found at the down standing leg of the upper outboard longeron. Further inspection using eddy current confirmed that the longeron was broken by 80% of the flange area. The strain gauge monitoring near the cracked location confirmed the changes of load path as well. Only the L/H side had a crack, the R/H side seemed not be cracked yet

During the Boeing FT01/ST16/FT93 tests this area was also severely damaged and had to be repaired by doublers several times. The ASIP pegging procedure could therefore not be applied for the estimation of the Swiss crack initiation life. The direct calculation of crack initiation life for the Swiss design spectrum showed a very low life. To meet the Swiss structural requirements of 10'000 FH crack initiation life Swiss interference fit fastener with LIF = 5 were recommended. The stresses at the upper outboard longeron in the test were high which would clearly lead to short initiation and crack growth life. A large stepped doubler was installed at the L/H side to ensure a by pass loading to avoid further damage, see Figure 4.2-14. During the repair all holes with removed fasteners were checked by eddy current, and more cracks were found. With this repair the test could be continued up to 10'400 FH without any further problems.

On the R/H side in the area of FS488 to FS499 up to the end of the test also some cracks were observed but none of them were very long and critical for the upper outboard longeron. Further checks and discussion showed that the LIF = 5 were not applied during the production due to impractical reasons. Therefore this longeron is highly loaded and a short life depending on the severity of the spectrum may be the case. This location must surely be analyzed more carefully for the fleet.

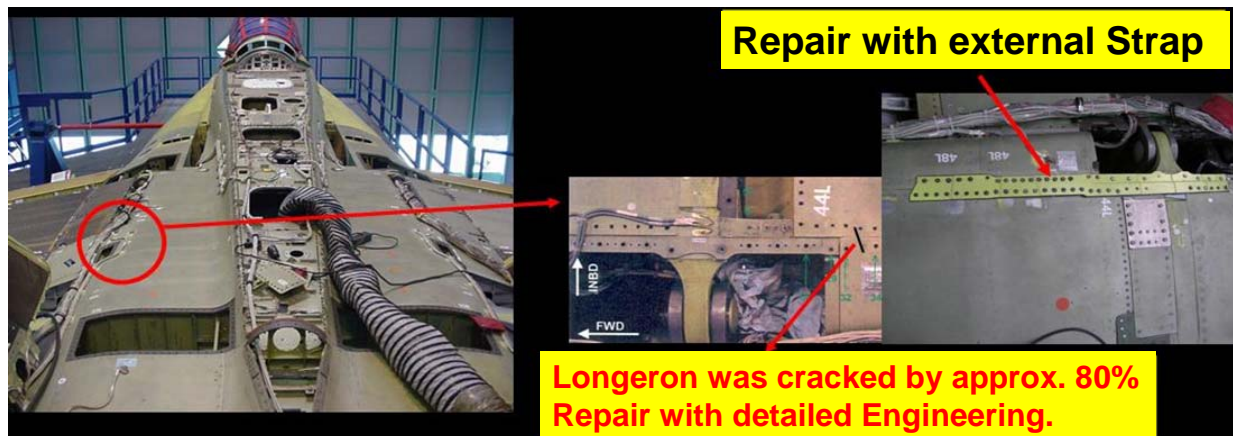


Figure 4.2-14 Cracked area of upper outboard longeron with strap repair.

*Failure at outboard TEF hinge rib on L/H side:*

The lug of Trailing Edge Flap (TEF) hinge rib at the L/H side showed a crack at 6'240 FH at the free edge corner. This part is maintenance critical and was not redesigned for the Swiss. This hinge rib is loaded highly by buffet during flight and therefore the ECP574 will also be introduced for the whole Swiss fleet. The replacement of the aluminium hinge rib for the fleet by a modified titanium hinge rib is already ongoing. The R/H side hinge rib was instrumented with strain gauges to monitor the spectrum loads. No changes were observed during the test.

The L/H rib failed at 6'606 FH in the test, see Figure 4.2-15. To understand why the rib failed detailed fractographic investigations were done. The results showed that drill marks were the origin of the crack. Once the crack has initiated the crack growth is pretty fast, so that no damage tolerance in fleet can ensure the structural integrity due to severe buffeting. For the Swiss test both ribs were replaced by the new titanium hinge rib to get strain gauge information for the new hinge rib by the Swiss test loads for further future stress analysis.

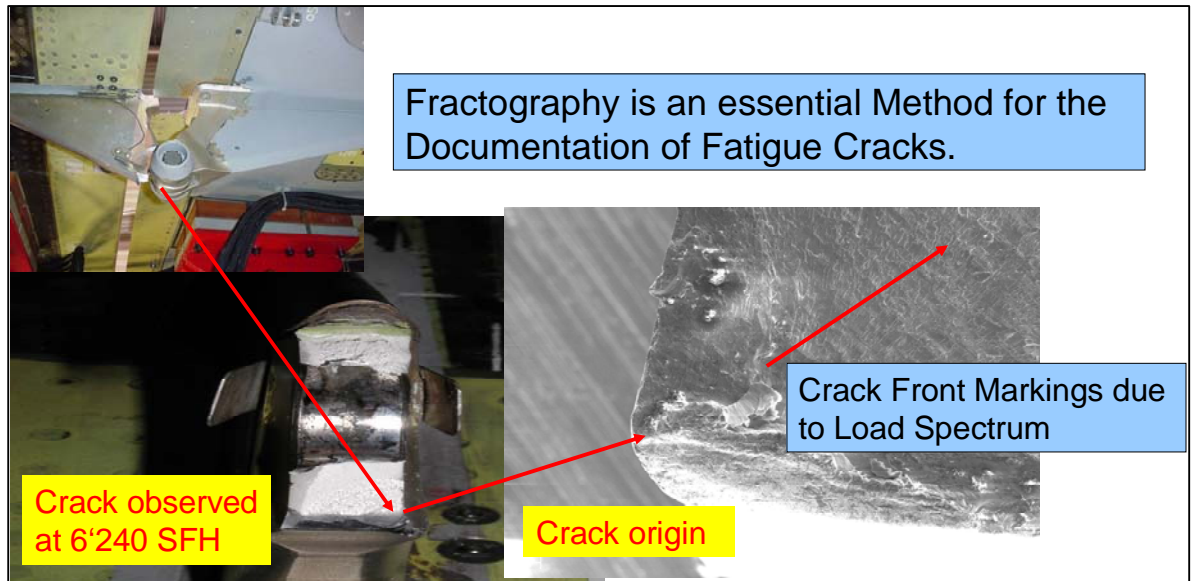


Figure 4.2-15 Failure of TEF flap at 6'606 FH, only on L/H side.

### 4.3 NEW MEASUREMENT TECHNOLOGY FOR DISPLACEMENT

M. Guillaume, RUAG Aerospace; G. Mandanis, M@M GmbH

To understand the three dimensional displacement of the whole airplane during the strain survey in the test rig of the F/A-18 RUAG Aerospace selected a new measurement technology.

The dimensional measurements were performed with the Krypton K-series optical metrology system. The measurements were carried out in August 2004 at RUAG Aerospace, in Emmen. The measurement and the post-processing of the data was done by Krypton, in Leuven (Belgium).

The purpose of the test was to record the displacements of the wings and the fuselage of the Swiss F/A 18. A total of 74 measurement points were defined. A full-scale test article had been used for this special measurement. Up to 9'000 FH had already been simulated. The most interest was to record the Z-displacement of the selected points, but the Krypton measurement system allowed to immediately record the 3D data of the requested points.

There were eight load cases simulated during the measurement. They are listed in Table 1. Every load case was applied in 15 steps. The initial and final step of each load case was 0% load.

N°	Load Case	Steps	Remark
1	TLC1496_1	15 from 0 to 70% and back	Strain Survey
2	TLC860	15 from 0 to 70% and back	Strain Survey
3	TLC525	15 from 0 to 70% and back	Strain Survey
4	TLC233	15 from 0 to 70% and back	Strain Survey
5	CHW001	15 from 0 to 70% and back	Strain Survey
6	CHF001	15 from 0 to 70% and back	Strain Survey
7	CHF002	15 from 0 to 70% and back	Strain Survey
8	TLC1496_2	15 from 0 to 70% and back	Strain Survey

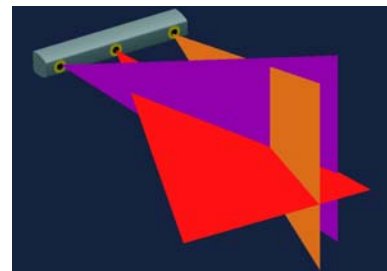
Table 1 The eight load cases.

The basis of the Krypton metrology system is the camera system, consisting of 3 linear CCD cameras.



The system itself relies on “active” LED’s for its functionality, which emit light in the infra-red spectrum. This light is invisible to the human eye but can be captured by the camera system, from which the computer can work out the LED’s exact position in 3D space.

The actual calculation of the position of the LED is done by comparing the images from the three linear CCD cameras. The middle camera ‘sees’ the longitudinal position of the LED, whilst the end cameras ‘see’ the transverse position. This has the effect of defining three separate planes on which the LED lies, the computer then calculates the intersection of these planes to give a position in 3D relative to the pre-calibrated camera.



Up to 1'000 LED's can be simultaneously tracked by the camera with the computer "strobing" the LED's so it knows which LED is 'on' at any time and this can be performed 1'000 times per second. This allows the software to 'over sample' measurements so as to remove any error. The ability to track multiple LED's in real time also allows the system to determine orientations of objects. By tracking the position of one LED on an object, its position in space can be determined in 3 dimensions. By attaching a second LED, the rotational position of the object is only constrained in one axis and therefore provides little extra information. It is only when a third LED is attached that a fixed plane can be defined. This then fixes the orientation of the object, therefore defining its position to 6 degrees of freedom.

Because of the size of the measurement object and the large deflection of the wing-tip, four Krypton camera's were used. Three K600\_8000 which were calibrated to measure up to 8 m, and one K600 which is calibrated to measure up to 6 m. An optimal configuration was studied to incorporate as many requested measuring points as possible. The coordinates were expressed in the global coordinate system (GCS) of the airplane (see below). For the orientations, the Roll-Pitch-Yaw convention was used: rotation order Z-Y-X and the rotations are performed around the absolute axis. Figure 4.3-1 shows a top-view of the set-up.

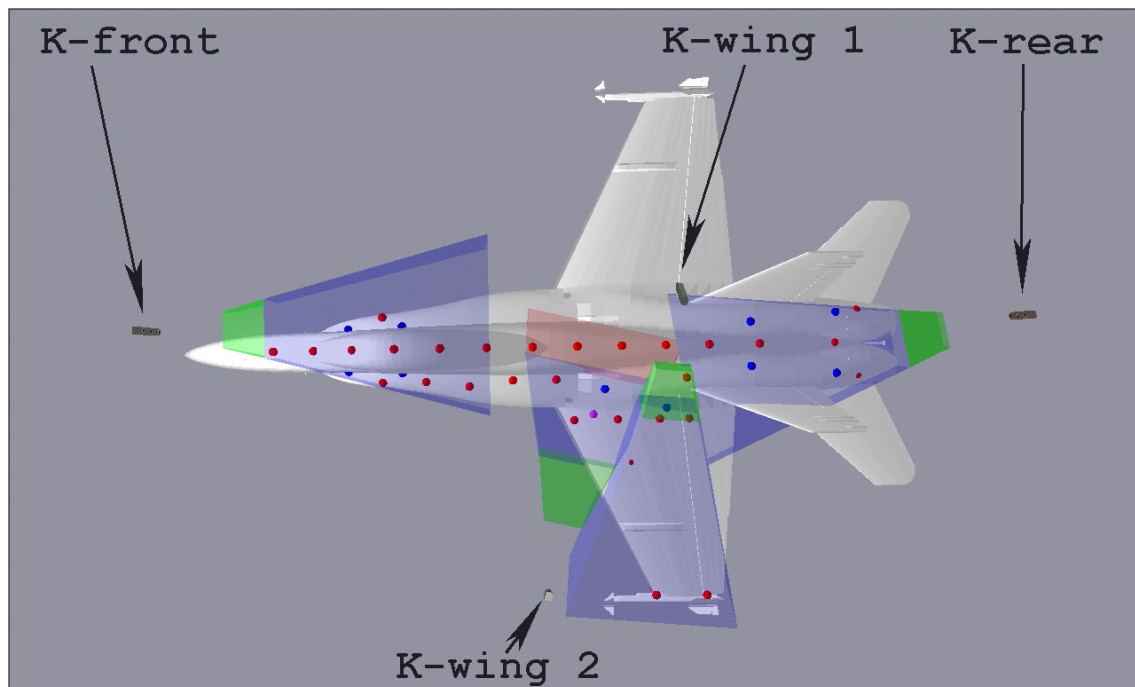


Figure 4.3-1 Top-view of the set-up.

Since these tests were viewed as a series of static measurements, calculations of the standard deviation of the results at each measurement condition should give a good idea of the accuracy of the measurements. The standard deviation figures were calculated for the duration of every sample interval for each step. The standard deviation is generally below 0.15 mm. Because of the reflections on the cockpit glass, the 6D antennas on the front of the airplane are less accurate.

Figure 4.3-2 gives an impression of the displacement of the TLC1496 load case. The displacement of the wing (amplification factor of 5) is clearly seen as bending and torsion. The aft fuselage shows also a relative big displacement compared to the forward fuselage.

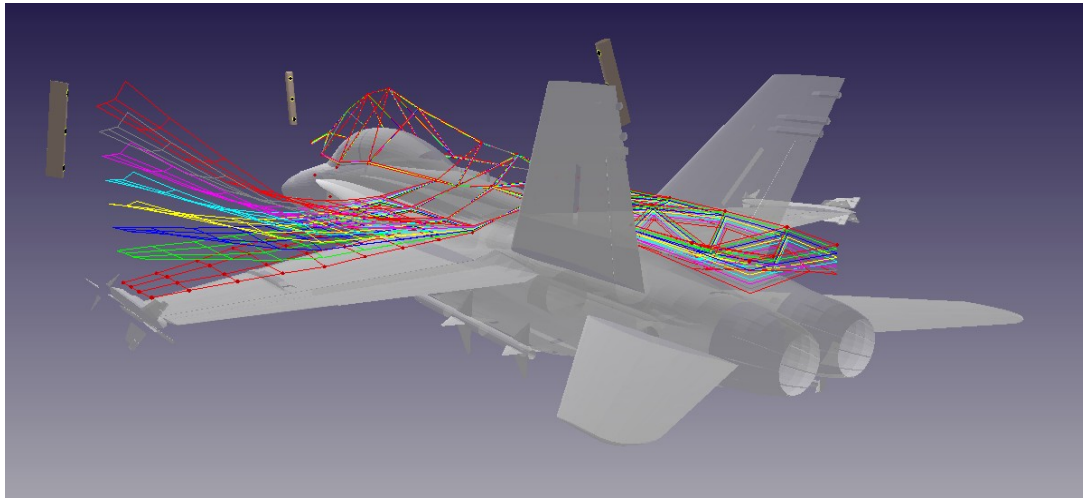


Figure 4.3-2 shows the displacement of the load case TLC1496 with the amplification factor of 5.

The evaluation of the data confirmed the vertical fuselage bending line related to the expected boundary condition at the restrained location of the landing gears. Asymmetric load cases showed a small torsion on the fuselage due to high stiffness.

The FREE LEX showed higher displacement at the same fuselage station compared to the fuselage. The forward fuselage showed small displacement compared to the aft fuselage section.

The linearity of the displacement in all three directions ( $x$ ,  $y$ ,  $z$ ) was checked for all measurement points and showed some deviations for the wing in  $y$  (side direction). The wing has a dihedral angle of  $3^\circ$  on the ground. Loading the wing by a flight condition induces a non linear  $y$  displacement which results first in a side slip outboard (at 10 to 30% load level) and afterwards inboard (at 40 to 70% load level). For detailed explanation see Figure 4.3-3.

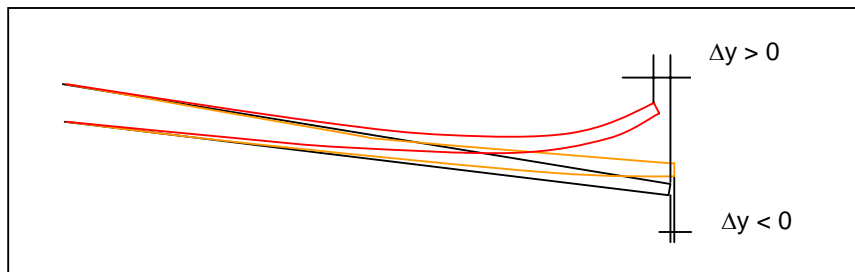


Figure 4.3-3 shows the influence of side displacement due to positive wing loading during strain survey.

## 4.4 FATIGUE LOADS DEVELOPMENT USING COMPUTATIONAL FLUID DYNAMICS

M. Guillaume, A. Gehri, RUAG Aerospace; J. Vos, CFS Engineering

### 4.4.1 Technology of Computational Fluid Dynamics

RUAG Aerospace has an inhouse multi modular block full Navier Stocks Computational Fluid Dynamics (CFD) Code so called NSMB. The code has no limitations on the number of blocks. A mesh of 8 million grid points was generated using the F/A-18 CAD data.

As an input for a steady state maneuver the following data is required: altitude, mach number (M), angle of attack, flap positions (leading edge flaps and trailing edge flap) and horizontal tail position. As a first step the grid mesh has to be adopted for the correct configuration. To reach a convergence about 3'000 iterations has to be done, see Figure 4.4-1.

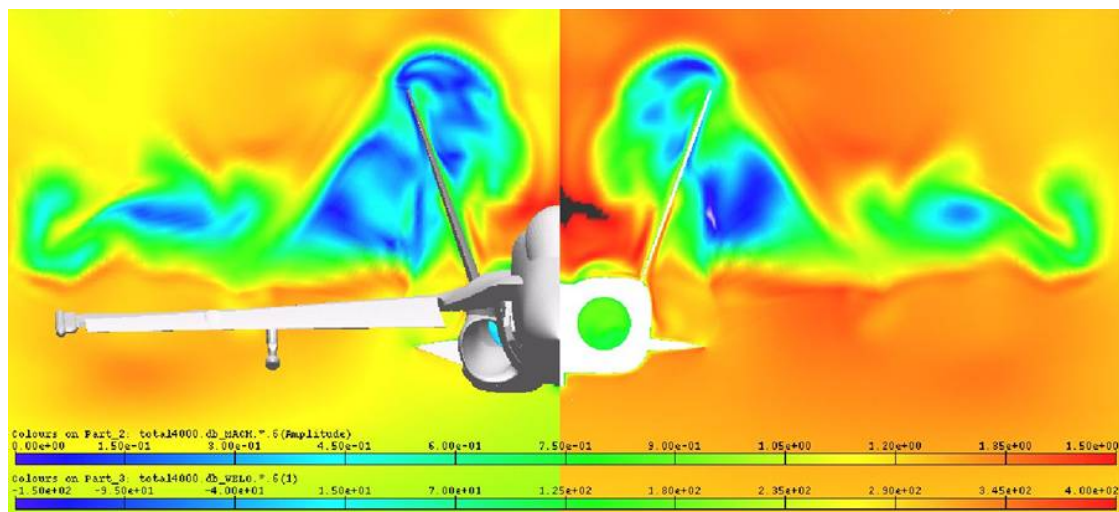


Figure 4.4-1 Calculation for steady state maneuver  $N_z = 8.25g$  at 25'000 ft and  $M = 0.95$  with AIM9 at the wing tip and one AMRAAM under each wing.

A post calculation was developed to calculate the loads for the various structural components at the load reference locations. For the wing the following loads were calculated:

- Wing Root Bending Moment, Torque, Shear
- Wing Fold Bending Moment, Torque, Shear
- Inboard Leading Edge Flap Hinge Moment
- Outboard Leading Edge Flap Hinge Moment
- Trailing Edge Flap Hinge Moment
- Aileron Hinge Moment

To validate the CFD calculations 15 symmetric load cases from the Boeing US Navy F4 flight loads data base were used. The component loads were in excellent agreement within a few percent.

Also 12 load cases from the Swiss ASIP study were also calculated. The results were also very good with the exception for the vertical and horizontal tail. For load cases with an angle of attack of less than 10 degrees the agreement was much better.

The structural deflection of the structure due to the stiffness was not considered. The deflection plays an important role for high normal  $N_z$  accelerations. Therefore a special force transfer tool was developed to transfer aerodynamic loads (CFD loads) to the grid of the structural finite element model (CSM). Then a finite element calculation was performed for the displacement of the structure (CSM). A second transfer tool has to be developed to transform the displacement of the CSM grid to the grid of the CFD model. Then the CFD mesh blocks has to be adapted to the displacement of the CFD surface grid. For details see Figure 4.4-2.

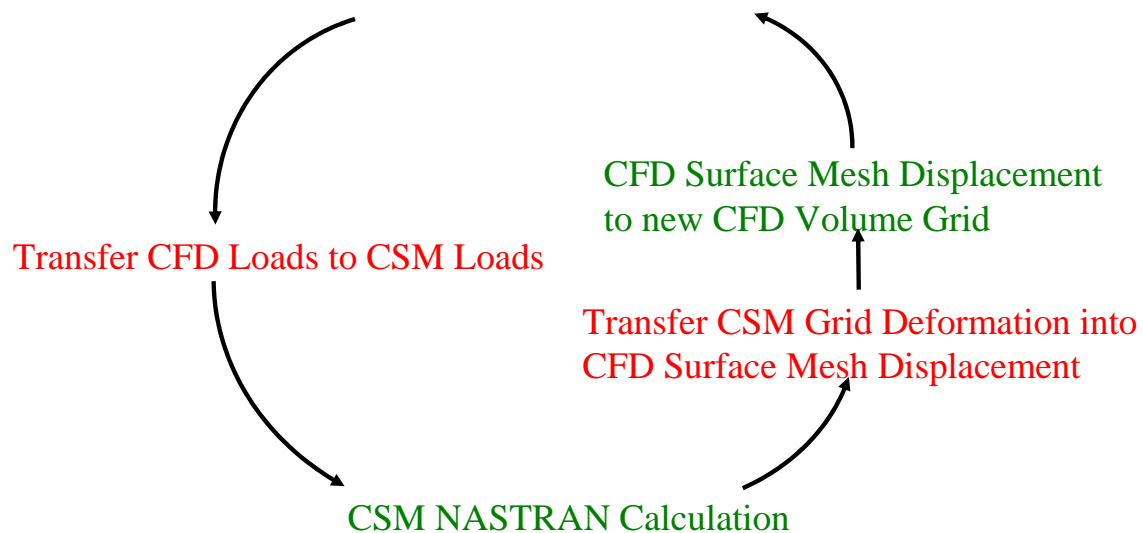


Figure 4.4-2 Iteration loop for calculation of CFD loads on flexible F/A-18 structure taking the stiffness into account.

The deflection of the structural components was calculated using the original F/A-18 finite element models. For 8.25g steady state pull up maneuver it just took for iterations to reach the convergence. The loads especially on the wing were reduced compared to the undeformed CFD calculation. RUAG calculations demonstrated that for high g maneuvers the stiffness of the wing structure has to be taken into account for fatigue loads development, see Figure 4.4-3.

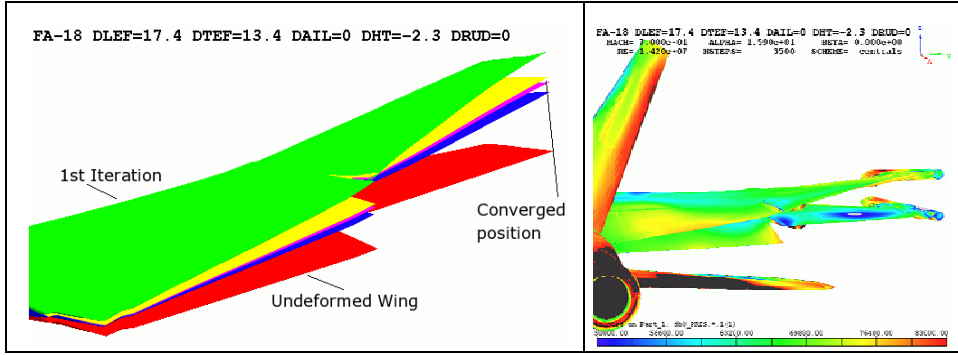


Figure 4.4-3 Influence of iterations on the wing displacement and final result with CFD plot.

RUAG also made a comparison between the displacement along the elastic axis of the wing between the full scale fatigue test (data measured by Krypton) and the CFD calculation taking the stiffness into account. The outer wing had a much higher bending moment (+ 18%) due to the actuator rod position discussed in the full scale fatigue test chapter. It is therefore not surprising that the CFD calculation showed a smaller displacement especially on the outer wing, see Figure 4.4-4. It is strongly recommend to fully understand the loading of the structure during a full scale fatigue test. The higher loading on the wing has surely an impact on the introduced fatigue damage during cycling. As mentioned in the full scale fatigue test chapter the fatigue life will be much shorter at critical locations compared to the design life of the ASIP study. Such an overtesting gives more margin of safety for the fleet which also could be expressed in higher safety factor compared to the factor of 2 used in the Swiss test.

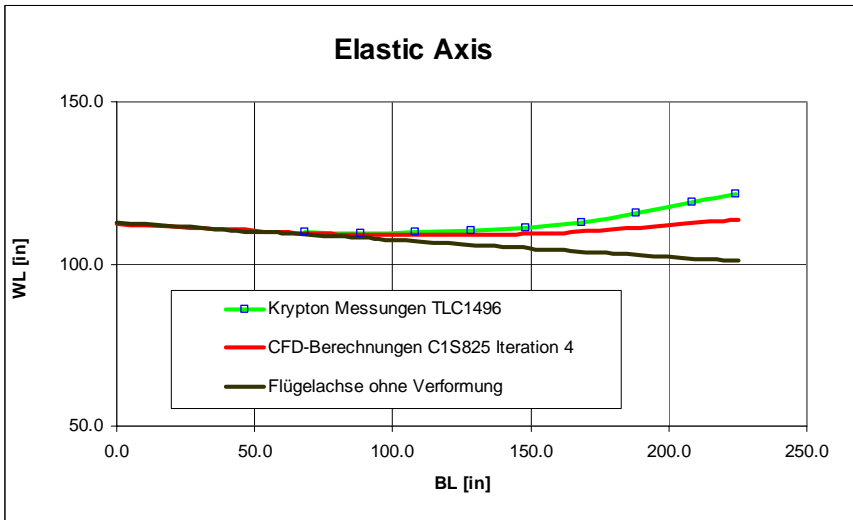


Figure 4.4-4 Comparison of F/A-18 wing displacement along elastic axis for test data, CFD result, and undeformed wing.

The RUAG Navier Stokes NSMB code is also able to calculate unsteady flow simulations. Therefore first calculations were done for unsteady state symmetric maneuvers of  $N_z = 4.5g$  and  $8.25g$ . For the load case of  $4.5g$  with an angle of attack of  $7.3^\circ$  no unsteady state flow was

observed. For the two load cases of 8.25g with an angle of attack of  $15.9^\circ$ , respectively  $26.6^\circ$  remarkable unsteady flow was predicted. The Figure 4.4-5 demonstrates clearly the difference in time at 0.2318 and 0.2718 sec for upper and lower part of the Figure. The result of the high dynamic loading on the aft fuselage is well known for buffet problems on the F/A-18 structure.

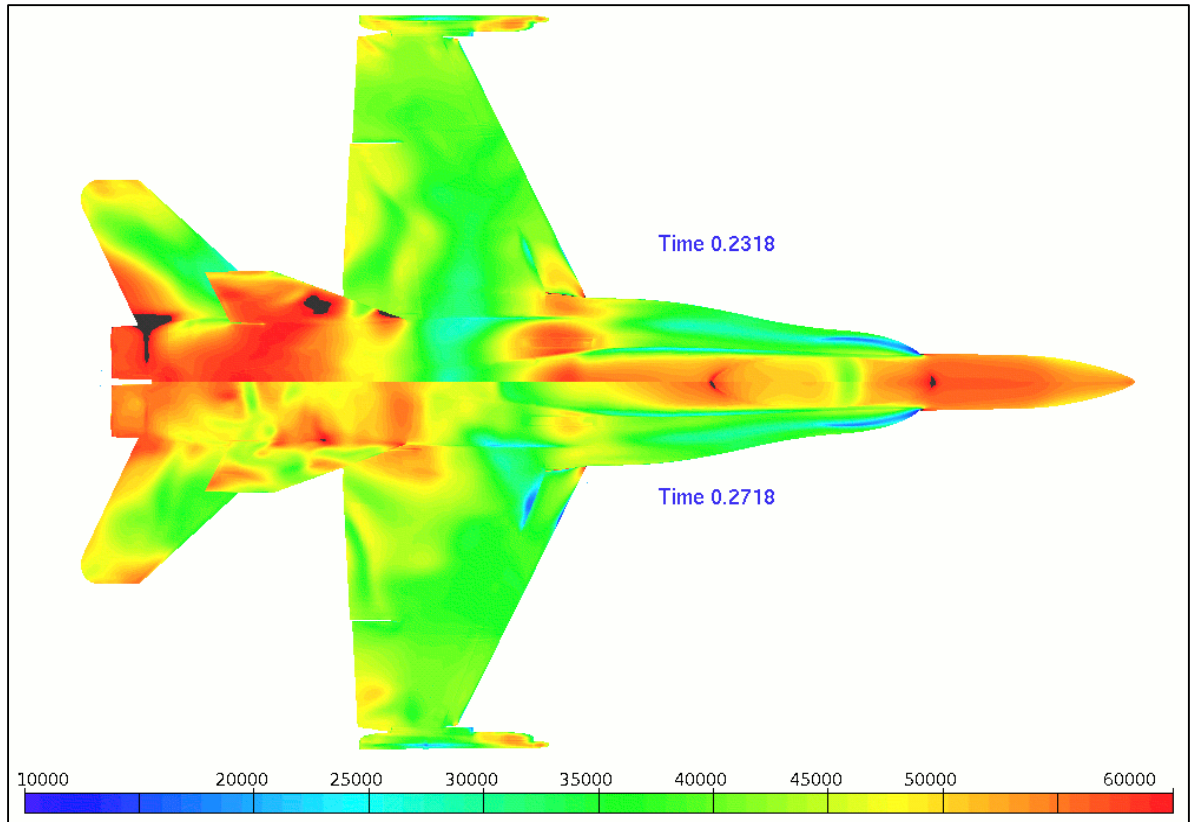


Figure 4.4-5 Unsteady CFD calculation for two time steps on the F/A-18.

## **4.5 FATIGUE RELATED TOPICS ON MILITARY AIRCRAFT**

### **4.5.1 Development of a Procedure to Calculate Aircraft Balanced Load Distribution for Swiss F/A-18 Service Flights**

St. Büsser, RUAG Aerospace

#### **Background**

All structural assessments for the Swiss F/A-18 Fleet and the Swiss F/A-18 full scale fatigue test refer to the Swiss Design Master Event Spectrum (MES). The usage survey of the Swiss F/A-18 fleet shows that to some extent the usage severity of the fleet is considerably different compared to the severity of the Swiss design spectrum. Durability analysis based on the Swiss Design MES may lead to too conservative results and to actions which are unnecessary or not necessary to that extent.

To be able to perform appropriate structural assessments for the Swiss F/A-18 fleet and to judge structural damages occurred in the Swiss F/A-18 full scale fatigue test the severity of the actual fleet usage must be taken in to account. The symmetric loads prediction (SLP) process has been developed to generate a usage spectrum based on the actual usage of the Swiss F/A-18 fleet for a selected zone of the fuselage.

A more detailed description of the SLP process and the loads derivation method was published in the ICAF national review 2003.

#### **Procedure and programs**

The Swiss usage spectrum comprises a set of approximately 200 selected usage flights. The characteristics of this spectrum represent the usage of the Swiss F/A-18 fleet. From each of this flights flight data reports recorded with the standard fatigue tracking software are available and used a data source for the SLP process.

To enable a simple and easy data processing a chain of various programs was developed. With the information from the flight data reports the maneuvers are identified and the corresponding set of the required input parameters for the SLP process are determined. For each maneuver the aircraft loads distributions are determined and balanced by applying the SLP process. The loads distributions are combined to a flight sequence and stored in one file per flight. Various plots are generated to enable an easy and quick assessment of the computed flight. A selection procedure allows to select some of the processed flights and to merge them to a usage spectrum.

#### **Extension of the range of application**

The initial version of the SLP process was only applicable to aircraft configurations without external stores. The only exceptions are AIM9 – missiles mounted on the wingtips. The usage survey of the Swiss F/A-18 fleet indicates that the aircraft is operated basically in an air-to-air weapons configuration with mounted centerline tank. To be able to process flights with centerline tank properly the configuration with centerline tank has been integrated in the SLP process.

#### **Validation and verification (V&V) of the SLP – process**

To answer the questions how reliable and precise the calculated results are, a verification and validation of the process was performed. In a first step single maneuver load cases with known loads distributions were analyzed and compared to the load distributions determined

with the SLP process. The two different load distribution were applied on FEM models and the calculated stresses were compared. As the identical load cases were applied on the full scale fatigue test some strain gauge measurements are available. The difference of the comparison of load distributions, calculated stresses and measured strains were very slight. To compare the SLP process with the Swiss design master event spectrum a subset of the Swiss Design MES was developed and processed with the design tools and the SLP process. Only symmetric maneuvers and flights with an air-to-air weapon configuration have been selected for this comparison. The match of the calculated CI life for several locations was convincing.

A total of 139 typical Swiss service flights (corresponds to 132 flight hours) were selected, processed and merged to a test spectrum which represents typical average severity of the Swiss F/A-18 fleet. The standard flight data reports include strain gauge measurements from two locations of the dorsal deck longeron and from one location of the canopy sill longeron. The predicted local stresses by the SLP process were compared to the measured strains. A detailed evaluation was performed and allowed gathering some additional experience with the SLP process applied in real environment. The evaluation showed good accordance.

#### 4.5.2 F/A-18, SLP, Load to Stress

B. Bucher, RUAG Aerospace

##### Introduction

Part of the stress sequence generation with SLP (Symmetric Loads Prediction) is the translation of discrete loads to a derived fleet FE model (FE4) of the Swiss F/A-18. With the loads processing tool slp\_mac loads along the fuselage reference stations and at the interface locations are generated from flight data load trends which are generated from different load sources. Figure 4.5-1 shows the role of the loads to stress calculation in the SLP process.

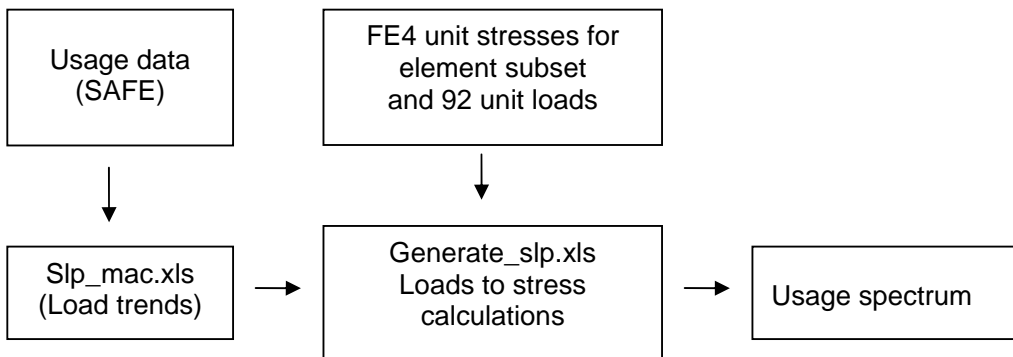


Figure 4.5-1 SLP process, data and data processing.

SLP is limited to the fuselage. Also, for every location limitations of accuracy must be accounted for due to the coarseness of the FE4 model and the locally applied external loads.

### Load application to the FE model

The discrete loads and moments are distributed to the structure with Nastran RBE3 elements. Those RBE3 elements don't add additional stiffness but translate a single load or moment to an equivalent load set. Loads are applied at a total of 80 grid points along the fuselage centre line and at the interface locations. Moments are applied at a total of 12 grid points to the structure at interface locations. The figure below shows the RBE3 elements which were used to spread discrete loads to the structure.

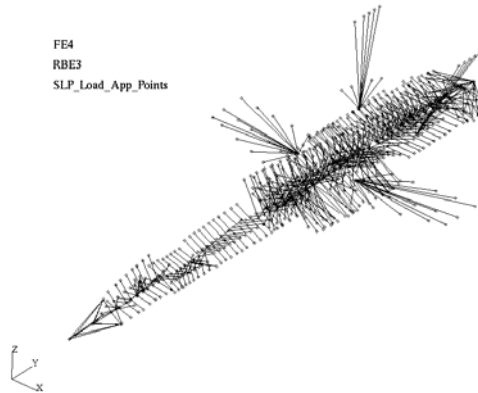


Figure 4.5-2 Nastran RBE3 elements used in FE4.

### Stress sequence generation using a unit load approach

On the FEM side it is sufficient to calculate the structural stress response once for 92 unit load cases for a selected element subset. Stresses then are calculated by linear combinations of the usage loads and the unit stresses. This calculation process has been automated using an Excel spreadsheet and visual basic code. For select locations verification checks have been performed. The verification checks can be summarized as follows:

- Load balance checks before and after application to FEM
- Stress checks for known load cases and elements with ASIP or ASIP-derived FE models
- Stress checks with strain gage data from the Swiss FSFT article FTS1
- Spectrum severity comparisons using the Swiss Design MES and the NGC Specgen process and SLP together with the FW\_Filter89 and the crack initiation software FW\_CI89

### Conclusion

The load to stress calculation is an efficient way to minimize CPU time of structural analysis FEM solvers and it allows translating flight loads data to stress sequences and therefore generate local element stress spectra. Estimating stress spectra based on known local load sequences e.g. the F.S. 383 fuselage bending moment sequence is not necessary anymore. Local effects are directly taken into account. SLP uses methods and FE models which are based on the Swiss F/A-18 ASIP study. Therefore similar accuracy can be expected. However, detailed stress spectrum during the ASIP study was only possible for the CTR/AFT Fuselage FEM SA0508. Now, with SLP and FE4 it is possible to generate spectra for the whole fuselage.

### 4.5.3 Development of Swiss F/A-18 Pegging Procedure

B. Bucher, M. Figliolino, RUAG Aerospace

In preparation for the Swiss F/A-18 FTS1 tear down inspection the pegging procedure adopted during Swiss F/A-18 ASIP study was revisited. No significant shortcomings could be identified.

Then it was investigated how results from the Swiss FTS1 full scale fatigue test could be used for an efficient and economic management of the Swiss F/A-18 fleet. It was concluded that the pegging procedure can be used for the following activities:

- Life predictions for fleet A/C based on FTS1 results
- Assessment of fleet damage by re inspection of FTS1 components
- Generation of new  $K_t$  DLS values for repair or redesign
- Assessment of potential for fleet life extension

Prerequisites to perform a pegging analysis according to our method are as follows:

- Full scale fatigue test data (configuration, cracks, strain gage data, spectrum)
- FE model of the FSFT article
- FE model of the fleet airplane
- Fleet usage data from an onboard A/C flight data monitoring system
- Fleet periodic inspection data

The full scale fatigue test data has been collected during the test of 10'400 SFH. Further data will be gathered during the FTS1 tear down inspection. The FE model of the test article (FE2) has been created during the engineering phase for the Swiss F/A-18 full scale fatigue test. In order to assess effects of over- and under testing another FE model (FE3) representing the fleet configuration and the fleet loads has been built. Flight data is constantly collected using the SAFE data acquisition system. The simplified process to translate flight data into local stress sequences using a specific version of FE3 (FE4) and known F/A-18 load trends from several sources is called SLP (Symmetric Loads Prediction). SLP has been described in the Swiss contribution to the ICAF 2003 country review.

The pegging process as it was applied is shown in the figure below.

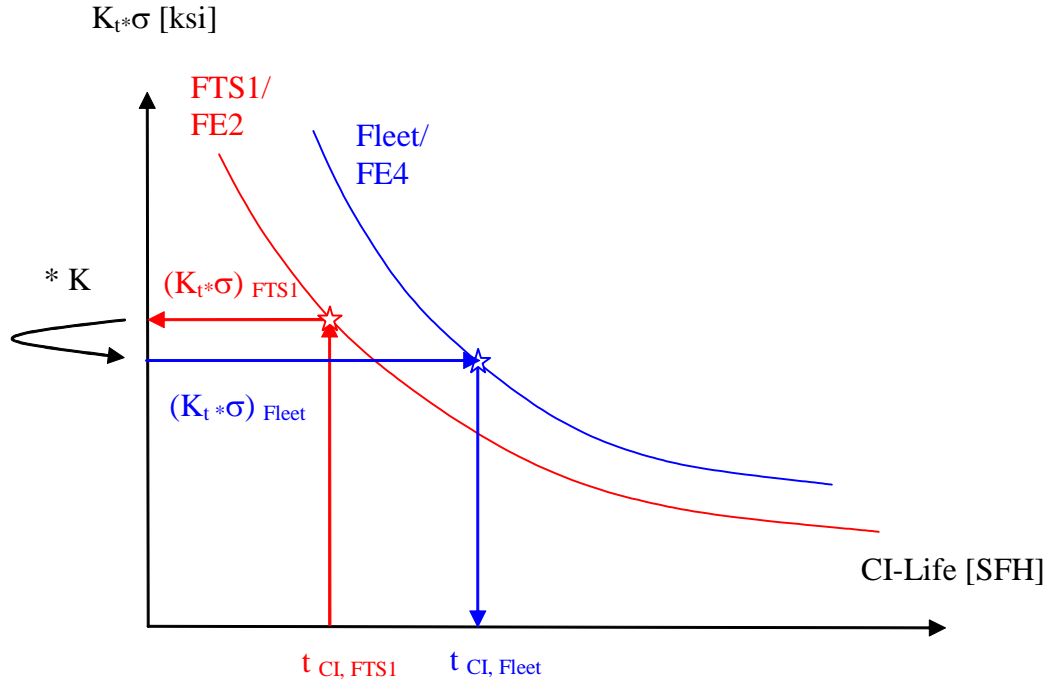


Figure 4.5-3 Prediction of crack initiation life for fleet usage

The factor  $K$  is a pegging factor which accounts for differences of stress concentration, cross section data and different reference stresses for the available spectrum data.

The red CI-Life Curve represents the FTS1 test article or if no direct measured strain gage data is available for the specific location the curve of the internal Loads FEM FE2 which represents the FTS1. The blue CI-Life curve represents the fleet usage data or if no flight data is available for the specific location the internal Loads FEM FE3 of the flying A/C configuration. For ease of application the FE3 FEM flaps deflections are all set to 0 degrees for all maneuvers of the aircraft.

The proposed pegging procedure has been demonstrated for 6 locations of interest on the F/A-18 structure.

### Coupon program- verification by test

#### Goal

Goal of the coupon program was to generate CI and CG data for a typical F/A-18 metallic material and for a preliminary Swiss fleet usage spectrum. The fleet usage spectrum was derived from all mission data available in the years 2001 and 2002 for the Swiss F/A-18 C Fleet. The fleet usage spectrum was derived from processed SLP usage data and the FE4 FEM Bar Element 470265. This FE element is located close to the wing root strain sensor in the Titanium bulkhead at FS470.5 at a location which is primarily dominated by the wing root bending moment.

The material chosen was Al-7050-T7451. For this material test data was already available from the F/A-18 FSFT work package WP 7600 when a selection of Aluminium and Titanium coupons were tested with the Swiss design spectrum (DESMES) and the test spectrum (MES6B5). Therefore it was possible to perform a spectrum severity comparison between the Swiss design spectrum and a preliminary Swiss usage spectrum based on coupon tests.

A total of 6 high  $K_t$  Coupons with a 6.5 mm centre hole were tested. The coupon is shown in the figure below.

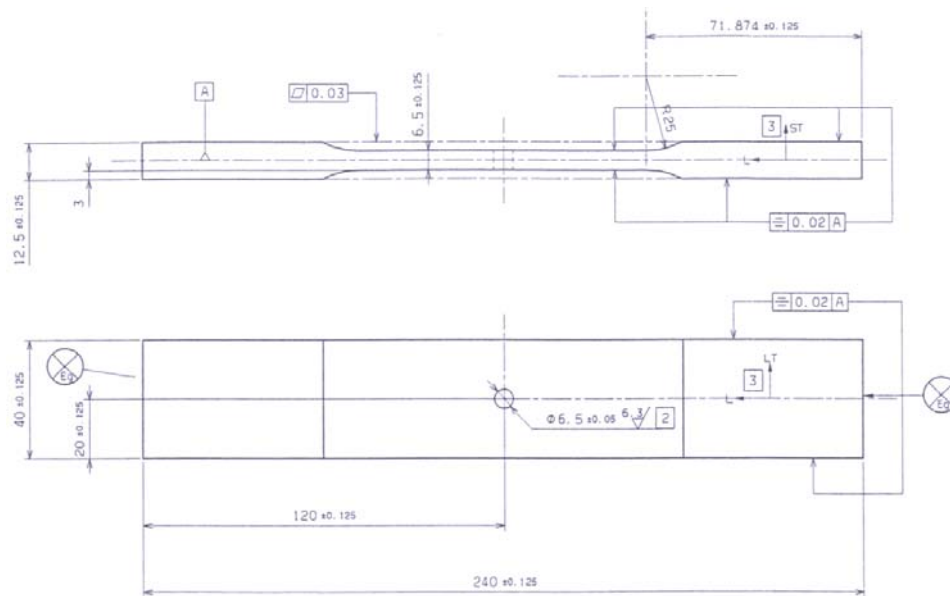


Figure 4.5-4 High  $K_t$  coupon Al 7050-T7451

#### Automated crack detection

Using a crack sensor crack initiation could be detected automatically with high confidence before corner cracks at the hole or surface cracks at the hole would grow beyond  $a = 0.25$  mm which by definition by Boeing is when CI occurs. Therefore the crack sensor is able to “measure” reasonably well CI Life. After detecting CI the coupon was further tested with the same spectrum to a nominal crack length of about 70% of the critical crack length of the coupon. After that the coupon was destroyed by increasing the load with a ramp of 1 respectively 2 mm/min. Using methods of fracture mechanics the apparent fracture toughness  $K_{app}$  was determined by analysing the fracture surface. A fracture model was identified in AFGROW which approximately matches the test results observed.

Since coupon tests for the same coupon configuration have been performed during the Swiss F/A-18 FSFT engineering work package WP 7600 the newly generated coupon data could be compared with this older data. Using the coupon test very similar severity factors compared to the engineering data with CI-Life curves using FW\_Filter89 and FW\_CI89 and Boeing material files could be found.

## Conclusions:

### Pegging procedure:

The baseline pegging procedures as utilized during the Swiss F/A-18 ASIP study may also be utilized for the post test and tear down analysis for an efficient fleet management.

### CI coupon test data:

- The coupon test results confirm that the preliminary Swiss usage spectrum is less severe than the Swiss design spectrum
- Life predictions with CI89 are conservative
- Due to a more sensitive crack sensor, cracks can be detected automatically before or at lengths of 0.25 mm

### CG coupon test data:

- During the crack growth phase usually several cracks are observed on the hole surface or at the hole corners
- Small cracks close to each other often grow together
- The ratio of  $CI_{\text{detected}} / (CI_{\text{detected}} + CG_{70\%})$  is 0.55
- The ratio of  $CI_{\text{detected}} / (CI_{\text{detected}} + CG_{90\%})$  is 0.62

The results above indicate that the rule of thumb: *Total Life = 2/3 CI Life + 1/3 CG Life* can also be adopted for the preliminary Swiss F/A-18 wing root bending moment usage spectrum. The total average automatically detected crack lengths using the crack sensor for Al-7050-T7451 was 0.22 mm.

## 4.5.4 Damage Investigation on F-5 Horizontal Stabilizer

A. Uebersax, M. Geering, RUAG Aerospace

Control surfaces of military fighter aircraft need special attention in design and repair. Stiffness requirements combined with reduced overall thickness and complex loading spectrum make these components demanding engineering workpieces.

In the year 2002 loose fasteners became apparent on several horizontal stabilizers of the F-5 Tiger fighter aircraft. The horizontal stabilizers of the F-5 are of a free floating design. They consist of an aluminum spar spliced to a steel fitting, aluminum honeycomb core with aluminum skin and aluminum closing rib. The fasteners, some of which were found to be loose, connect the aluminum skin with the steel fitting in the root area of the stabilizer. Additionally to the fasteners, the skin is also bonded to the steel fitting.

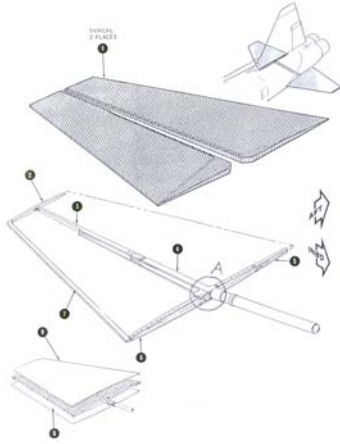


Figure 4.5-5 Structure of F-5 horizontal stabilizer.

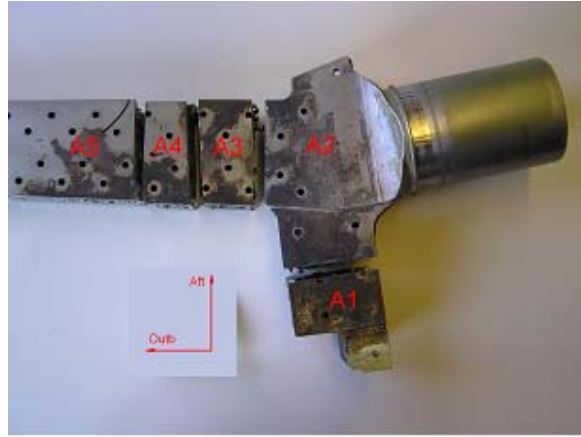


Figure 4.5-6 Corroded steel fitting, sectioned during teardown inspection.

This type of damage, getting a fleet wide problem within the Swiss Air Force F-5 fleet, called for more in-depth investigations on one hand and for immediate actions on the other hand.

Teardown inspection on 3 stabilizers was conducted. In all 3 stabilizers extensive damage was found in the root region. The disbonds between the steel fitting and the skin were revealed to be of an adhesion failure type on the steel fitting. The steel fitting itself started to corrode, as well as the adjacent aluminum honeycomb. In some small areas the honeycomb core revealed fatigue cracking. Also 2 of the 3 stabilizers showed fatigue cracked closing ribs.

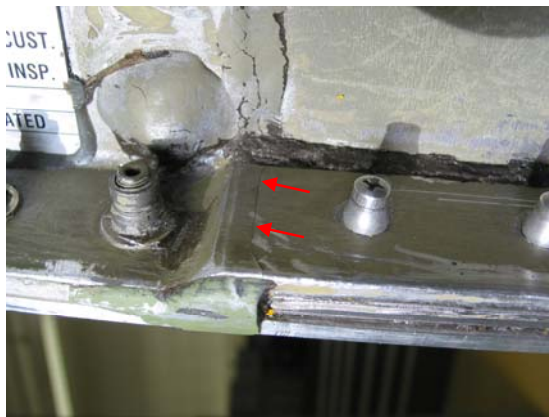


Figure 4.5-7 Cracked closing rib.

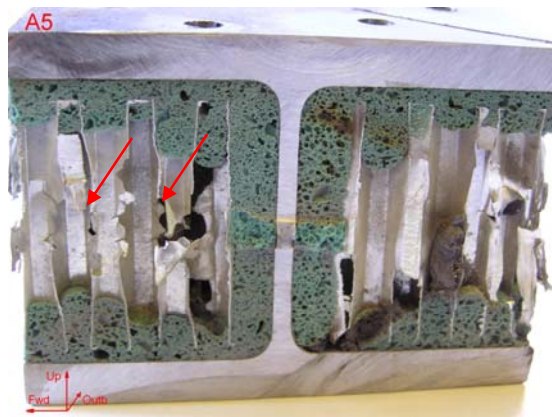


Figure 4.5-8 Corroded and cracker honeycomb core.

A finite element model (FEM) of the horizontal stabilizer was built. The model is as much detailed as to provide accurate results for single fasteners in the root region. An abrupt pitch maneuver loadcase at 5'000 ft Mach 0.88 proved to produce the highest stresses in the bondline and on the fasteners in the root region.

Based on the findings of the teardown inspections and the finite element model, the most probable failure mechanism was evaluated, which consist of an adhesion failure between the skin and the steel fitting, followed by loosening fasteners and secondary damages to the

honeycomb core, corrosion on the steel fitting, failure of the closing rib and failure of the fasteners, leading finally to a loss of the horizontal stabilizer.

Knowing all these facts, an interim repair for certain damage sizes was determined. The repair consists of the replacement of 7 PLT-110-6 fasteners per side by PLT-150-6 or PLT-150-8 fasteners, depending on the size of the disbanded area.

The repair was analyzed by finite element modeling and adapted crack growth analysis for the steel fitting. Stiffness of the stabilizer was checked analytically with different damage sizes and the corresponding repairs. Additionally to the analysis, a static residual strength test was conducted to validate the interim repair. Results were in accordance with the predicted failure mode.

The interim repair was introduced in the Swiss Air Force fleet with an adapted non destructive inspection concept for the stabilizers assuring safety of flight. This kind of interim repair helps to guarantee fleet availability and readiness until all defect horizontal stabilizers are replaced.

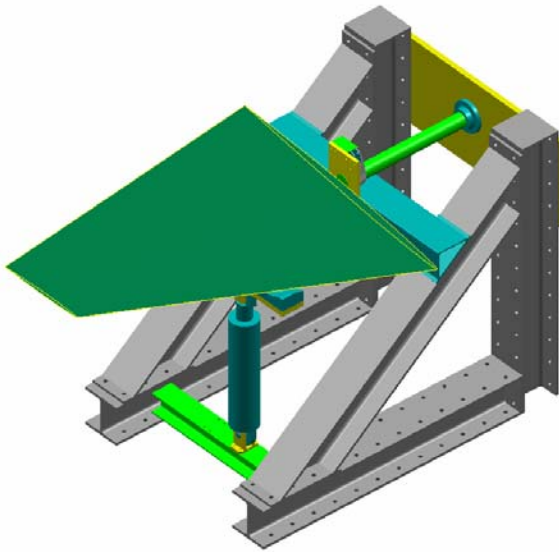


Figure 4.5-9 Layout of static residual strength test.

## 4.6 FATIGUE RELATED APPLIED RESEARCH AND DEVELOPMENT

### 4.6.1 Repair Welding of Titanium Parts

M. Nievergelt, M. Geering, RUAG Aerospace

The use of large and complex integral parts in modern lightweight structures results in increased efforts if these parts need to be replaced. Increased costs and down time, associated with the replacement of these parts, result directly from high component costs, long delivery periods and additional labour due to the great number of mating points with the surrounding structure. Therefore, in most cases, the repair of a damaged part is more economical and faster to accomplish than part replacement. In addition to well known repair methods, repair by welding may have a high economical potential in certain aerospace applications when technical feasibility can be demonstrated.

Repair by welding is not an issue for structural parts made of aluminum alloys due to their poor weldability and use in heat treated conditions. Modern lightweight structures often embody parts made of titanium alloys to ensure the fatigue life requirements, e.g. the three Carry-Through-Bulkheads and Dorsal Longerons of the Swiss F/A-18C/D model.

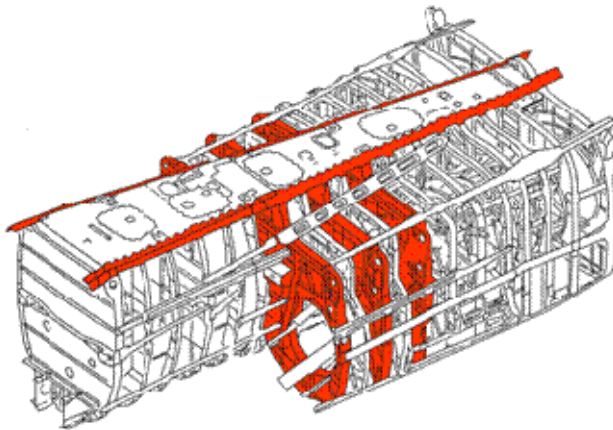


Figure 4.6-1 Structural Titanium parts (shown red) in the Swiss F/A-18C/D center fuselage.

In service, typically only non-structural titanium parts, such as heat shields, are repaired by welding. The salvage of machined titanium parts by welding during production is possible. However, a furnace heat treatment is required in order to ensure a proper microstructure and the relief of residual stresses within the weld and heat affected zone (HAZ).

Ti-6Al-4V offers a good weldability and is often used in the annealed condition. In service repairs by welding might be feasible. However, a furnace heat treatment would require the removal of the part, eliminating a considerable amount of the benefit of repair versus replacement. To perform an in situ weld-repair of structural parts without furnace heat treatment is questionable and a poor fatigue performance is expected. However, as a weld-

repair may be applied more than one time, a significant shorter fatigue life compared to the baseline life may still be acceptable. A first test result exceeded the expectations by far and more research was launched. The goal of the study was to obtain more information in order to advance titanium welding techniques and to evaluate whether weld repairs are applicable for structural titanium parts.

The study's focus was to determine the fatigue behaviour (crack nucleation and crack growth life) of weld-repaired specimens compared to baseline specimens. As literature indicated that the HAZ might have worse properties than the weld itself, the HAZ was addressed as well.

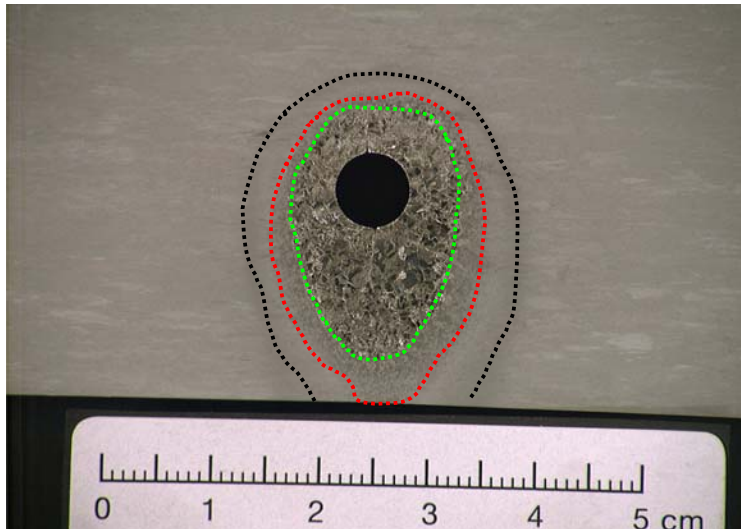


Figure 4.6-2 Typical macrostructure of a welded joint.  
Circled in green: welded material, circled in red: coarse grain zone of the HAZ, circled in black: end of the HAZ.

In order to gain practical experience, the test specimens were loaded with the Swiss F/A-18 design wing root bending moment (WRBM) spectrum. Two stress levels were chosen such that the baseline configuration reached a so called crack initiation (CI) life of 2'500 and 5'000 flight hours respectively, marking out the second half of the Swiss F/A-18 planned service life. Earlier fatigue damages are considered unlikely, whereas later ones are no longer relevant. In order to cover the range of practical stress concentrations, two  $k_t$  factors were used (center hole in a plate coupons,  $k_{tg} = 3.2$  and 'shallow gradient' coupons,  $k_{tn} = 1.5$ ). In order to allow a minimal statistical evaluation, a set of 5 coupons was tested with the same set of parameters.

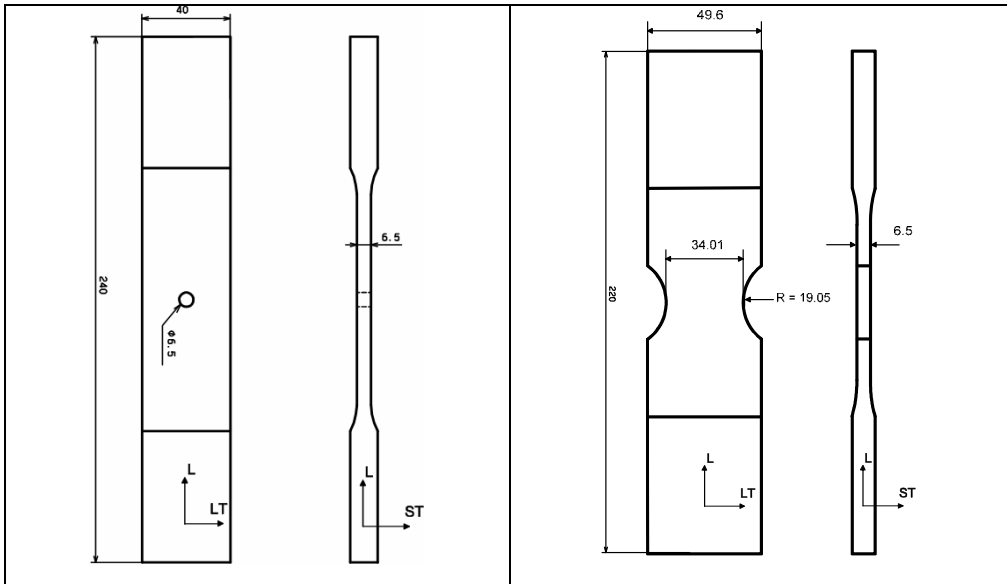


Figure 4.6-3 Coupon Geometry

F/A-18 WRBM Swiss Design MES, Ti-6AL-4V RA Plate						
High $K_t$ ( $K_{tg} = 3.24$ )			Low $K_t$ ( $K_{tn} = 1.5$ )			
	Baseline	Weld	HAZ	Baseline	Weld	HAZ
$\sigma_{2'500}$	5	5	4	n/a	n/a	n/a
$\sigma_{5'000}$	5	5	3	5	5	n/a

Table 4.6-1 Test Matrix

In order to explain large variations of the fatigue behaviour, the microstructure of the weld and the HAZ of selected specimens were metallographic analyzed and correlated to the welding parameters that were used.

A thermal non stationary, non linear finite element model (FEM) was created in order to evaluate the influence of different weld parameters. Thermal results and stress results obtained by the FEM were compared to test results.

The feasibility of a local in situ heat treatment by inductive heating and simultaneous water cooling was addressed. Due to its universal applicability, the tungsten inert gas (TIG) welding method was used. However, since this method turned out to be hard to carry out with a good repeatability, alternative welding methods were taken into consideration.

The test results show that the weld is generally more critical than the HAZ. The lives of the weld show a larger variation than the lives of the baseline and the HAZ. The average lives of the weld and the HAZ are in the range of 23% to 76%, compared to the average baseline lives. The results of the study indicate that the repair of structural titanium parts by welding might be an alternative for certain aerospace applications. However, in order to set up a qualified repair process, a large amount of further investigation needs to be done.

**Total Life of High Kt Sigma 5000 Tests  
(WRBM SD)**

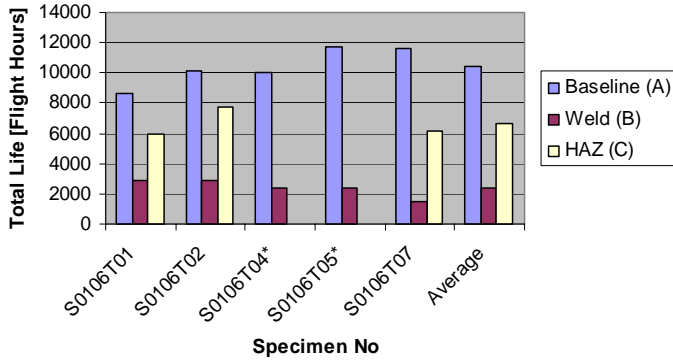


Figure 4.6-4 Total Life Results of the High Kt Sigma 5000 Tests.

**Total Life of High Kt Sigma 2500 Tests  
(WRBM SD)**

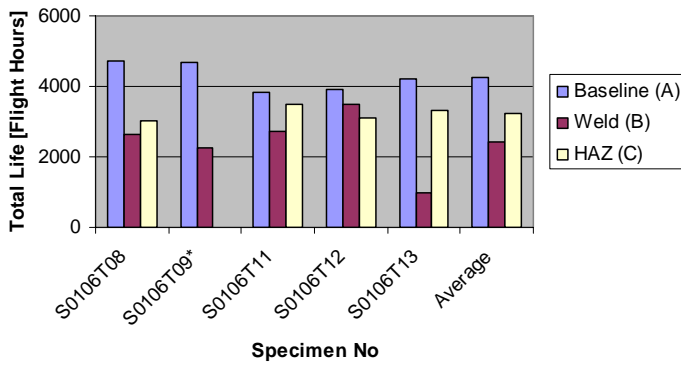


Figure 4.6-5 Total Life Results of the High Kt Sigma 2500 Tests.

**Total Life of Low Kt Sigma 5000 Tests  
(WRBM SD)**

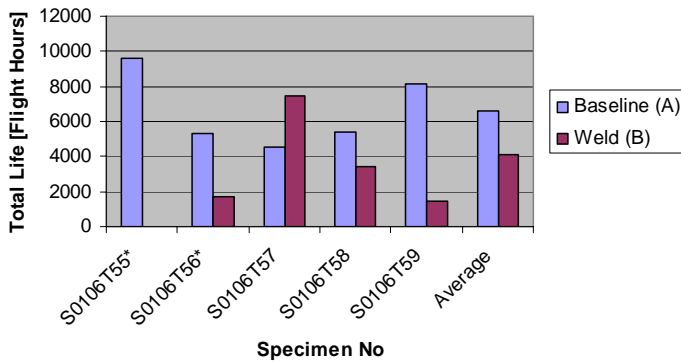


Figure 4.6-6 Total Life Results of the Low Kt Sigma 5000 Tests.

## 4.6.2 Fatigue Behavior of Metals and Residual Stresses

M. Geering, A. Uebersax, RUAG Aerospace

### Introduction

Recently a research program has been started to evaluate fatigue behavior of metals in conjunction with residual stresses. The program is divided in two major subjects: Introduction of residual stresses by pre-stressing and relaxation of residual stresses by vibratory stress relief (VSR). General objective of the program is to improve fatigue life of metal parts through improved residual stress processing.

Tensile residual stresses may reduce the performance or cause failure of manufactured products. They may increase the rate of damage by fatigue, creep or environmental degradation. They may reduce the load capacity by contributing to failure by brittle fracture, or cause other forms of damage such as shape change or crazing. Compressive residual stresses are generally beneficial, but cause a decrease in the buckling load.

Residual stresses may be measured by non-destructive techniques, including X-ray diffraction, neutron diffraction and magnetic and ultrasonic methods; by locally destructive techniques, including hole drilling and the ring core and deep hole methods; and by sectioning methods including block removal, splitting, slicing and layering.

Prediction of residual stresses by numerical modeling of welding and other manufacturing processes has increased rapidly in recent years.

Allowing for residual stresses in the assessment of service performance varies according to the failure mechanism. It is not usually necessary to take account of residual stresses in calculations of the static strength of ductile materials. Design procedures for fatigue or buckling of welded structures usually make appropriate allowances for weld-induced residual stresses, and hence it is not necessary to include them explicitly. Residual stresses have a major effect on fracture in the brittle and transitional regimes, and hence the stress intensity,  $K$ , or energy release rate,  $J$ , due to residual stresses must be calculated and included in the fracture assessment.  $K$  or  $J$  may be obtained as a function of stress distribution, crack size and geometry by various methods, including handbook solutions, weight functions, and finite element analysis.

### Pre-stressing

Pre-stressing which is a kind of cold working, results in the movement or slip of crystal lattice imperfections that create dislocations in metals. Cold working increases the density of dislocations, which ultimately reduces available slip systems, and results in the strain hardening of metals. During this process, the crystal lattice of a metal becomes strained as a result of added dislocations.

The idea is to pre-stress a part in the same manner as it is stressed during service, but with higher stress amplitude. Basically the same techniques are well known as autofrettage in pressure vessel and piping industry.

The goal within this subject is to model the process and predict the fatigue life and therefore finally determine the optimal amount of pre-stress required for specified specimen geometry. Special attention will be given to the Bauschinger Effect which will influence fatigue life considerably once mixed tension and compression spectrum loading will be applied.

**Vibratory Stress Relief (VSR)**

Manufacturing processes such as welding, machining and casting often cause a build up of stresses in components. These stresses must be relieved because they add to the service stresses and thereby may increase the susceptibility of the components to distortion or failure. Vibratory Stress Relief (VSR) is a general term used to refer to the reduction of stresses by means of cyclic loading treatments. A commonly applied VSR treatment involves vibration of a component to achieve high stress amplitudes. VSR is looked as an economic substitute to thermal stress relieving.

This process of VSR avoids the disadvantages of thermal stress relief and may be applied at any point during the manufacturing process. The potential savings in time, equipment and energy costs are substantial.

Today, the exact mechanism of VSR is still not completely understood. It is believed that VSR alters the residual stresses of second and third order, what has been demonstrated by neutron diffraction measurements. The goal of the project is to evaluate the effect of VSR treatment and altering residual stresses of second and third orders on the fatigue life.

Specimen fatigue tests are under way to evaluate effects of the resonant vibratory stress relief (R-VSR) on crack initiation and crack growth life in 7050-T7451 aluminum alloy. A series a non VSR treated and VSR treated high  $K_t$  specimens with and without cold worked holes are tested. Included are also residual stress measurements by neutron diffraction.

**4.6.3 Automated Crack Detection by Crack Sensor**

S. Zehnder, RUAG Aerospace

On high  $K_t$  specimens, dynamically generated cracks of length  $a = 0.25\text{mm}$  are detected automatically using the crack sensor developed by RUAG Aerospace. The sensor can be used on a servo hydraulic test system with single-stage, block-program or spectrum loading. It can detect both, surface corner cracks as well as surface cracks inside boreholes. If the eddy current signal exceeds the critical signal level, the test system will stop immediately. With this kind of crack sensor, crack initiation (CI) tests can be performed much more economically.

During development of the eddy current crack sensor, several tests have been carried out to evaluate the sensitivity of the sensors.

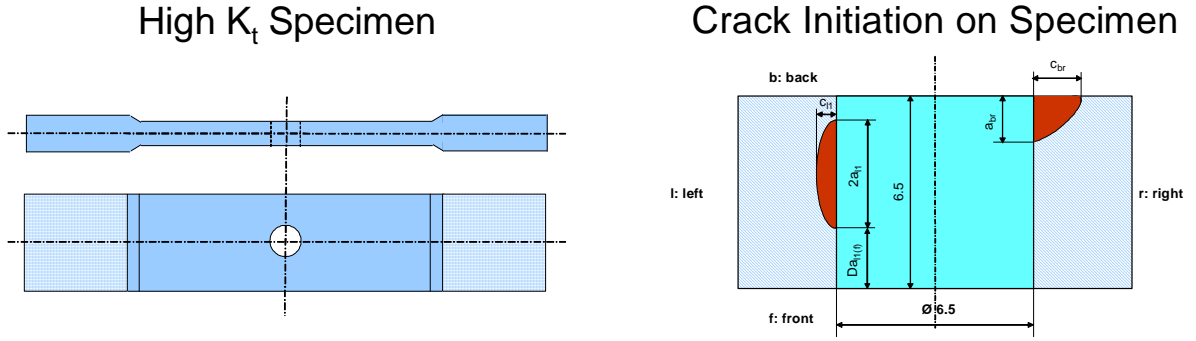
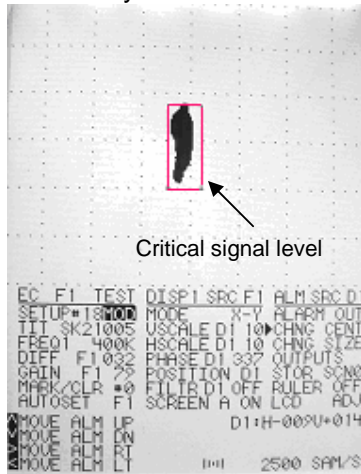


Figure 4.6-7 Typical specimen and crack description used.

Average Sigma Gross Max [Mpa]	Max. Value crack length a Specimen Nr. 1	Max. Value crack length a Specimen Nr. 2	Max. Value crack length a Specimen Nr. 3	Average CI Crack Length [mm]
226	0.135	0.20	0.44	<b>0.26</b>
197	0.155	0.21	0.18	<b>0.18</b>

Table 4.6-2 Extract of generated test data using Al-7075-T7451 specimens.

Display Screen of the Eddy Current Instrument



Cracksensor

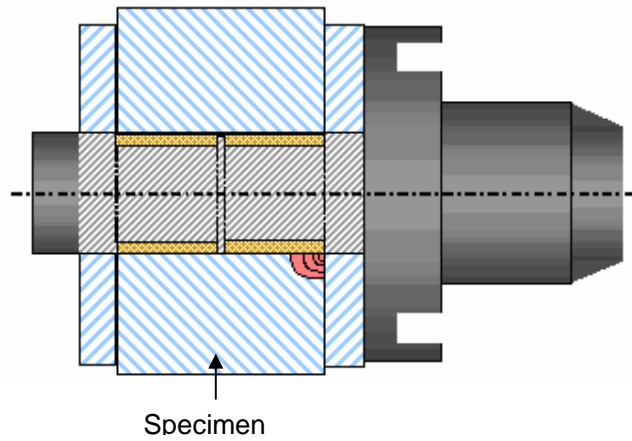


Figure 4.6-8 Eddy current signal and eddy current probe.

Requirements for the eddy current device:

- High signal sensitivity and stability
- Small temperature drift
- Low-noise digital instrument
- Movable alarm window
- Logic alarm output

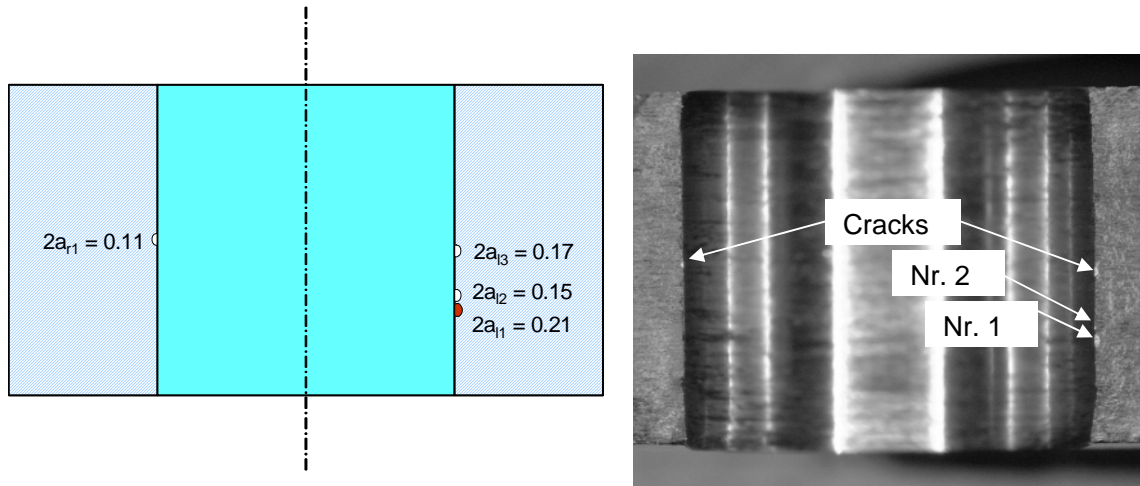


Figure 4.6-9 Force opened specimen after crack sensor exceeded critical signal level. The initiated multiple cracks were evaluated fractographically. Indicated crack lengths are by optical microscope.

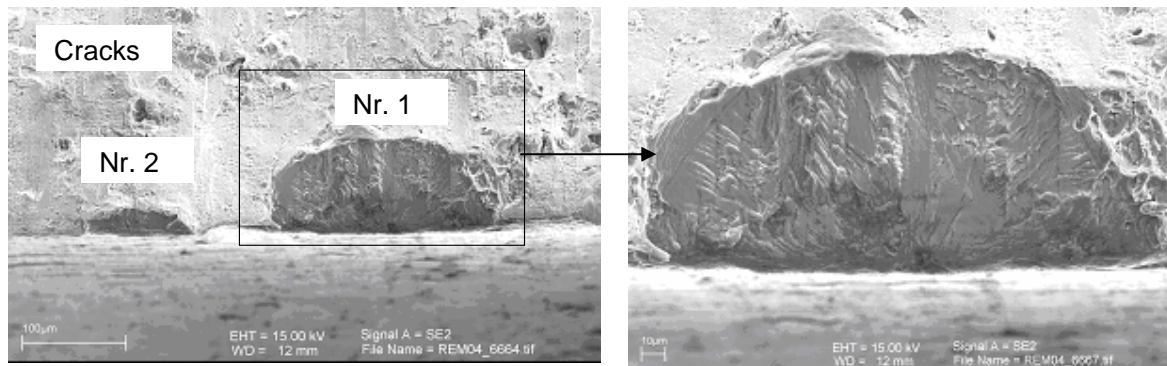


Figure 4.6-10 Pictures of initiated cracks by scanning electron microscope SEM.

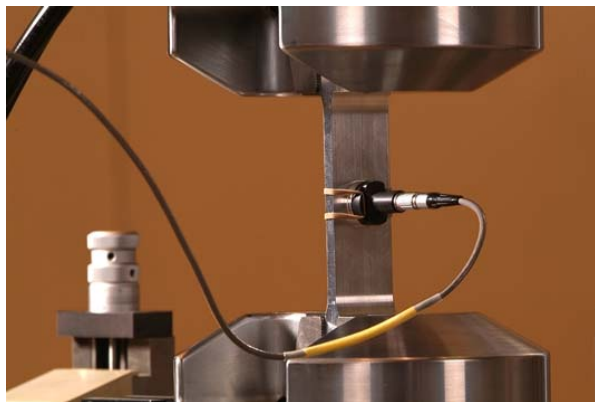


Figure 4.6-11 Crack sensor in place on test specimen.

## 4.7. FULL SCALE FATIGUE TEST OF THE PILATUS PC-21 AIRCRAFT

N. Rössler, D. Haenni, Pilatus Aircraft Ltd.

### 4.7.1 Introduction

The Pilatus PC-21 trainer is a low-wing monoplane (Figure 4.7-1) with a pressurized stepped, tandem-seat cockpit. It's powered by a 1'600 HP turboprop engine. The aircraft is designed to satisfy the needs of the basic and the advanced pilot training. In addition to the high aerodynamic performance, it is equipped with a mission computer, which has more capacity than any other found in current generation training aircraft.



Figure 4.7-1 PC-21 Trainer.

The primary structure of the aircraft is made of aluminum alloy in machined and sheet form. The aircraft has to meet an operational load factor range of +8g and -4g for symmetric maneuvers. The required service life is 15'000 flight hours for the PC-21 design spectrum.

### 4.7.2 Full Scale Fatigue Test Program

In order to certify the airplane to FAR 23, a full scale fatigue test (FSFT) must be conducted. This FSFT must also comply with damage tolerance requirements of MIL-81227. The goals of this test are:

- To demonstrate the economical life of the aircraft, which should be greater than the design service life of 15'000 flight hours.
- To verify previously determined fatigue critical locations based on engineering approaches and determine new fatigue critical locations based on FSFT results.
- To verify the damage tolerance capability of the airframe, in order to assure safe operational usage during the service life of the aircraft.
- To determine inspection intervals and appropriate inspection methods.
- To certify structural redesigns and repairs, in case cracks appear in an early stage of the test.

An airframe, representing the production standard, will be tested in order to perform a representative FSFT. The test article consists of the entire fuselage with the engine mount, the wing and the vertical tail. The horizontal tail as well as the landing gears are dummy structures. The test article is equipped with 180 strain gauges and 6 deflection transducers.

The test will be conducted with 24 push/pull actuators. The actuator loads are mainly applied to whiffletrees, which introduce the loads to the test article by means of loading pads and contour boards. The loading pads on the wing are located on the upper skin to insure an accurate load introduction and to get better access to the critical wing locations for inspection.

The test spectrum is derived from the master design spectrum (see 22<sup>nd</sup> Symposium of ICAF, "Fatigue Development Program for the PC-21 Trainer Aircraft"). It consists of 3 types of missions, 22 distinct design sorties, 36 unique types of maneuvers and 69'129 events. The spectrum represents a block of 500 flight hours. In order to shorten the test duration of the FSFT, the number of events of the master design spectrum was reduced to 58'035 events. This was done based on an analytical approach to insure that the two spectra create the same damage in the major structural parts, such as wing and fuselage.

In order to test the aft fuselage in a realistic manner, a vertical tail side load spectrum was developed and integrated into the FSFT spectrum.

The spectrum block of 500 flight hours will be repeated 90 times during the FSFT to simulate 45'000 flight hours, in order to fulfill the:

- durability test of 30'000 simulated flight hours,
- and the final damage tolerance test of 15'000 simulated flight hours.

The serial PC-21 will be equipped with a Health Unit & Monitoring System (HUMS). This system allows collecting data of the service spectrum of each aircraft. A comparison of these spectra with the FSFT spectrum will be possible at a stage later.

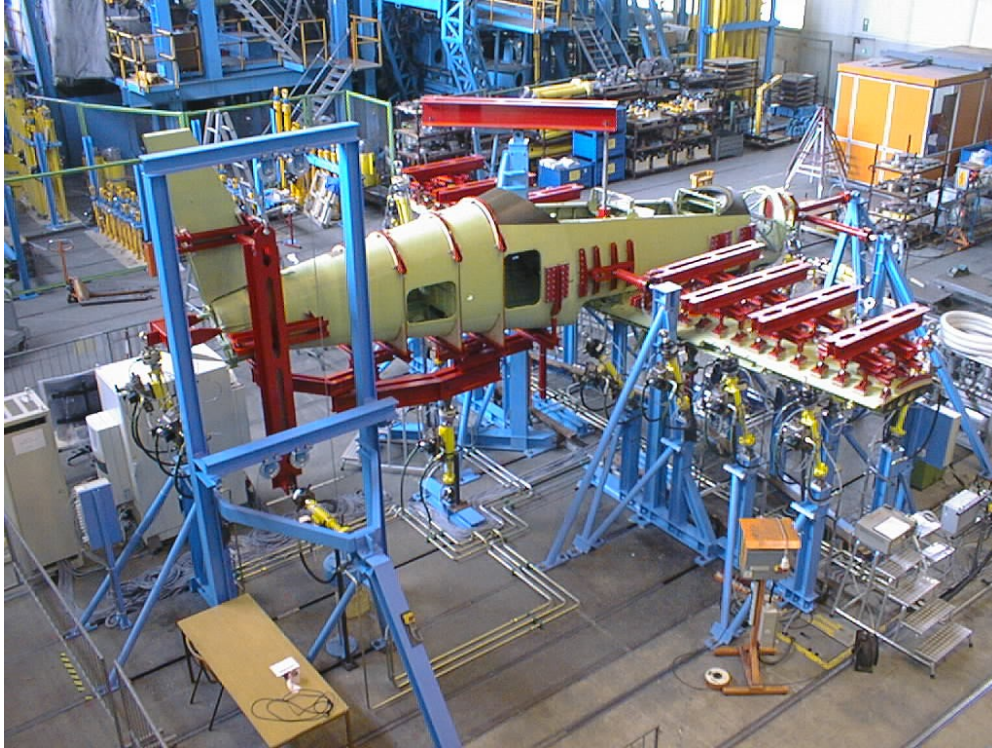


Figure 4.7-2 PC-21 Full scale fatigue test set-up at IABG Ottobrunn.

The FSFT will be performed at the test facility of IABG in Ottobrunn, see Figure 4.7-2. The FSFT starts immediately after the ICAF 2005 conference and will be probably run until spring 2006.

For the ICAF 2007 a presentation of the PC-21 FSFT test results is planned, which will be compared with the first collected data of HUMS.